Annual Review of Fluid Mechanics

Convection in Lakes

Damien Bouffard[1] and Alfred Wüest[1,2]

[1]Department of Surface Waters Research and Management, Eawag (Swiss Federal Institute of Aquatic Science and Technology), CH-6047 Kastanienbaum, Switzerland; email: damien.bouffard@eawag.ch, alfred.wueest@eawag.ch

[2]Physics of Aquatic Systems Laboratory (Margaretha Kamprad Chair), Institute of Environmental Engineering, École Polytechnique Fédérale de Lausanne, CH-1015 Lausanne, Switzerland

Annu. Rev. Fluid Mech. 2019. 51:189–215

First published as a Review in Advance on September 5, 2018

The *Annual Review of Fluid Mechanics* is online at fluid.annualreviews.org

https://doi.org/10.1146/annurev-fluid-010518-040506

Keywords

bioconvection, buoyancy-driven flows, double diffusion, shear-induced convection, surface convection, thermobaric instability

Abstract

Lakes and other confined water bodies are not exposed to tides, and their wind forcing is usually much weaker compared to ocean basins and estuaries. Hence, convective processes are often the dominant drivers for shaping mixing and stratification structures in inland waters. Due to the diverse environments of lakes—defined by local morphological, geochemical, and meteorological conditions, among others—a fascinating variety of convective processes can develop with remarkably unique signatures. Whereas the classical cooling-induced and shear-induced convections are well-known phenomena due to their dominant roles in ocean basins, other convective processes are specific to lakes and often overlooked, for example, sidearm, under-ice, and double-diffusive convection or thermobaric instability and bioconvection. Additionally, the peculiar properties of the density function at low salinities/temperatures leave distinctive traces. In this review, we present these various processes and connect observations with theories and model results.

1. INTRODUCTION

In this review, we refer to convection as motions that result from the action of gravity upon an unstable density distribution in a fluid. Convective mechanisms in lakes are no different from equivalent processes in other geophysical environments; therefore, study of convection benefits from research in related fields such as oceanography (Soloviev & Lukas 2014), planetary boundary layer dynamics (Emanuel 1994, Mellado 2017), earth and star interior processes, and even astrophysics (Miesch & Toomre 2009, Garaud 2018). Convection partly controls mixing and stratification of the water column and thereby drives vertical fluxes and transport. The key source of convection is the buoyancy flux, B, defined by

$$B(z) = -\frac{g}{\rho} F_\rho(z), \qquad 1.$$

where z is the vertical upward axis parallel to gravity with origin at the air–water interface, and where $F_\rho(z) = \overline{\rho' w'}(z) + \alpha\rho D_T \frac{\partial T}{\partial z} - \beta\rho D_S \frac{\partial S}{\partial z}$ is the density flux (**Table 1**). α and β are respectively the thermal expansion and salinity contraction coefficients; D_T and D_S are

Table 1 Key physical parameters used in the text

Symbol (units)[a]	Definition and equation	Typical values
α (K^{-1})	Thermal expansion coefficient: $\alpha = -\rho^{-1}\left(\frac{\partial\rho}{\partial T}\right)$ Approximation (T in units of °C): $\alpha(T) = 10^{-6}\left(-65.4891 + 17.12544T - 0.178155T^2\right)$	$\alpha < 0$ for $T < T_{MD}$ $\alpha > 0$ for $T > T_{MD}$
β (‰)	Saline contraction coefficient for the local specific salt composition of concentration C: $\beta = -\rho^{-1}\left(\frac{\partial\rho}{\partial C}\right)$	$\beta \approx 0.807 \times 10^{-3}$ for $Ca(HCO_3)_2$
ε ($W\ kg^{-1}$)	Rate of dissipation of turbulent kinetic energy	10^{-12}–10^{-6}
ρ ($kg\ m^{-3}$)	Water density (see the sidebar titled Density of Inland Waters)	1,000
B_0 ($W\ kg^{-1}$)	Surface buoyancy flux: $B_0 = \frac{g}{\rho}\left(\frac{\alpha}{C_p}H_{Q_0} - \beta H_{S_0} - \beta_P H_{P_0}\right)$	10^{-10}–10^{-8}
B_* ($W\ kg^{-1}$)	Effective buoyancy flux: $B_* = \frac{1}{h_{CML}} \int_{-h_{CML}}^{0} B(z)dz$	10^{-10}–10^{-7}
D_T ($m^2\ s^{-1}$)	Molecular diffusivity for heat	$\sim 1.4 \times 10^{-7}$
D_S ($m^2\ s^{-1}$)	Molecular diffusivity for salinity	$\sim 2 \times 10^{-9}$
A	Entrainment coefficient: $A = Ri_\Delta E$, with $Ri_\Delta = -\frac{h_{CML}\Delta b}{w_*^2}$, and Δb is the buoyancy jump across the entrainment layer	~0.1–0.3
E	Entrainment rate: $E = \frac{1}{w_*}\frac{\partial h_{CML}}{\partial t}$	10^{-4}–10^{-1}
h_{CML} (m)	Convective mixed layer thickness	10^{-3}–10^{2}
H_E ($W\ m^{-2}$)	Latent heat flux	Lake Constance: 20 (spring) to 70 (summer)
H_C ($W\ m^{-2}$)	Sensible heat flux	Lake Constance: −10 (spring) to 30 (summer)
H_{LW} ($W\ m^{-2}$)	Net longwave radiation	Lake Constance: −150 (fall) to 150 (spring)
H_{Q_0} ($W\ m^{-2}$)	Net surface heat flux (without H_{SW})	−200 (day) to 200 (night)

(*Continued*)

Table 1 (*Continued*)

Symbol (units)[a]	Definition and equation	Typical values
H_{SW} (W m^{-2})	Shortwave solar radiation: $H_{SW}(z) = H_{SW}(0)e^{-k_d z}$	0–1,000
H_{S_0} (kg m^{-2} s^{-1})	Net surface salt flux	10^{-5} in extremely salty lakes
k_d (m^{-1})	Attenuation coefficient of downwelling irradiance: $k_d(z) = -\frac{1}{z_2 - z_1} \ln \frac{H_{SW}(z_1)}{H_{SW}(z_2)}$	Turbid lake: $\mathcal{O}(1)$ Clear lake: $\mathcal{O}(0.1)$
L_{MO} (m)	Monin–Obukhov length scale: $L_{MO} = u_*^3/kB_0$ $z < L_{MO}$: shear stress–driven turbulence $z > L_{MO}$: buoyancy-driven turbulence	Large range: $\mathcal{O}(10^{-1})$–$\mathcal{O}(10)$
N^2 (s^{-2})	Local water column stability (N is the Brunt–Väisälä frequency): $N^2 = -\frac{g}{\rho}\frac{\partial \rho}{\partial z}$	10^{-10}–10^{-1}
Ra	Rayleigh number: $Ra = \frac{g\alpha \Delta T \delta^3}{\nu\kappa}$	$Ra > \mathcal{O}(10^3)$: development of convective instabilities $Ra > \mathcal{O}(10^6)$: turbulent convection
R_ρ	Density ratio: $R_\rho = (\beta \Delta S/\alpha \Delta T)^{\pm 1}$ (+ for the diffusive regime and – for the finger regime)	Layering for $1.5 < R_\rho < 6$
T_{MD} (°C)	Temperature of maximum density [z (m) positive upward]: $T_{MD}(z) \approx 3.984 + 0.0021z$	$T_{MD} = 3.984$°C at the water surface for $S = 0$ ‰
u_* (mm s^{-1})	Friction velocity in water	0.5–5
w_* (mm s^{-1})	Convective scale velocity: $w_* = (B_* h_{CML})^{1/3}$	Under ice: 1–7 Free surface cooling: 1–50
z_C (m)	Compensation depth: $k_d H_{SW}(z_C) = \frac{H_{Q_0}}{z_C}$	For $H_{Q_0} = 50$ W m^{-2} and $H_{SW}(0) = -500$ W m^{-2}, $z_C \approx 0.5$ m with $k_d = 0.2$ m^{-1} and $\approx$0.1 m with $k_d = 1$ m^{-1}

[a]Symbols without corresponding units denote dimensionless quantities.

respectively the molecular diffusivity for heat and salinity. F_ρ usually resumes to $F_\rho(z) = \overline{\rho' w'}(z)$, that is, the local covariance of the vertical velocity w' and density fluctuations ρ', except when molecular diffusion plays a role, such as under strong stratification or for double diffusion (DD). For the convective processes discussed in this review, B is always a source of turbulence, and much of the research concerns how $F_\rho(z)$ can be expressed as a function of bulk parameters.

What distinguishes convection in lakes from that in other geophysical environments? All environmental fluids are characterized by a wide range of processes acting at different temporal and spatial scales that must be distinguished to adequately quantify their associated rates and fluxes. Wind stress, and associated shear-driven mixing, often perceived as the strongest external forcing, is typically at least one order of magnitude weaker over lakes than over the ocean, while surface heat fluxes, for instance, are comparable (at a similar geographical location). Consequently, convective processes in lakes are usually distinctively observable. Thus, this review examines the main convective processes documented, yet often neglected, in lakes and differs from previous review articles that have focused on stratified lakes with an emphasis on internal waves and shear-induced turbulence (Csanady 1975, Imberger & Hamblin 1982, Wüest & Lorke 2003).

DENSITY OF INLAND WATERS

The oceanographic equations of state are not applicable for almost all inland waters, due to their very low salinity S (‰) of typically less than 1 ‰ (g kg^{-1}) and their different ionic compositions (more double-charged ions compared to ocean water). For the potential density $\rho(T)$ of pure water, we recommend using the temperature (T) dependency by Tanaka et al. (2001). For low-salinity natural waters, the density formula $\rho(T, S)$ by Chen & Millero (1986) can be used, and we recommend the general procedure explained in Wüest et al. (1996) for the haline contraction coefficient β. For the most common constituent $Ca(HCO_3)_2$, $\beta = 0.807 \times 10^{-3}$ ‰ (Boehrer & Schultze 2008). The additional density contributions from particles (Sánchez & Roget 2007) and gases (Schmid et al. 2004b) can be added linearly by using their corresponding β values. As by far the largest portion of the inland waters have low T and S, the use of the density function near the temperature of maximum density T_{MD} is the most critical for convective processes in lakes. The T_{MD} for freshwater is 3.9839°C at the water surface and decreases with pressure p (bar) and salinity according to

$$T_{MD}(S, p) = 3.9839 - 0.019911\,p - 5.822 \times 10^{-6} p^2 - (0.2219 + 1.106 \times 10^{-6} p)S,$$

whereas the density increases as

$$\rho_{MD}(S, p) = 999.972 + 4.94686 \times 10^{-2} p - 2.0918 \times 10^{-6} p^2 + (0.80357 + 1 \times 10^{-4} p)S.$$

In this review, priority is given to observations of convection in inland waters, and thus it does not include the pioneering laboratory and modeling studies that have contributed tremendously to the understanding of convection. The historical spatial and temporal undersampling of in situ observations is less of an issue today with the development of high-frequency instrumentation for profiling systems, distributed moorings, and underwater vehicles. Yet, with buoyancy-driven flows in lakes, it remains important to accurately estimate the density field in natural waters and associated fluxes resulting from temperature (T), salinity (S), suspended particles (P), and gases (see the sidebar titled Density of Inland Waters).

2. CONVECTION INDUCED BY BOUNDARY FLUXES

In this section, we review the convective turbulence occurring at the boundaries of lakes as a result of external fluxes that lead to gravitational instabilities (**Figure 1**). The application of Equation 1 defines the boundary buoyancy flux B_0 (W kg^{-1}), which is composed of the relevant turbulent boundary fluxes, such as heat H_{Q_0} (W m^{-2}), salinity H_{S_0} (kg m^{-2} s^{-1}) and suspended particles H_{P_0} (kg m^{-2} s^{-1}) (see **Table 1** for the definition of symbols used):

$$B_0 = \frac{g}{\rho}\left(\frac{\alpha}{C_p} H_{Q_0} - \beta H_{S_0} - \beta_P H_{P_0}\right). \qquad 2.$$

2.1. Surface Thermal Convection

The largest source of buoyancy fluxes consists of the thermal fluxes between water and the atmosphere, and the signs of these fluxes change following daily and seasonal regimes. For $B_0 > 0$, the lake is prone to penetrative cooling that causes mixing and deepening of the surface layer by heat loss ($\alpha > 0$). This process, usually dominant at night, controls the near-surface thermal structure (Imberger 1985). Cooling plays a key role in lacustrine biogeochemical cycling, among

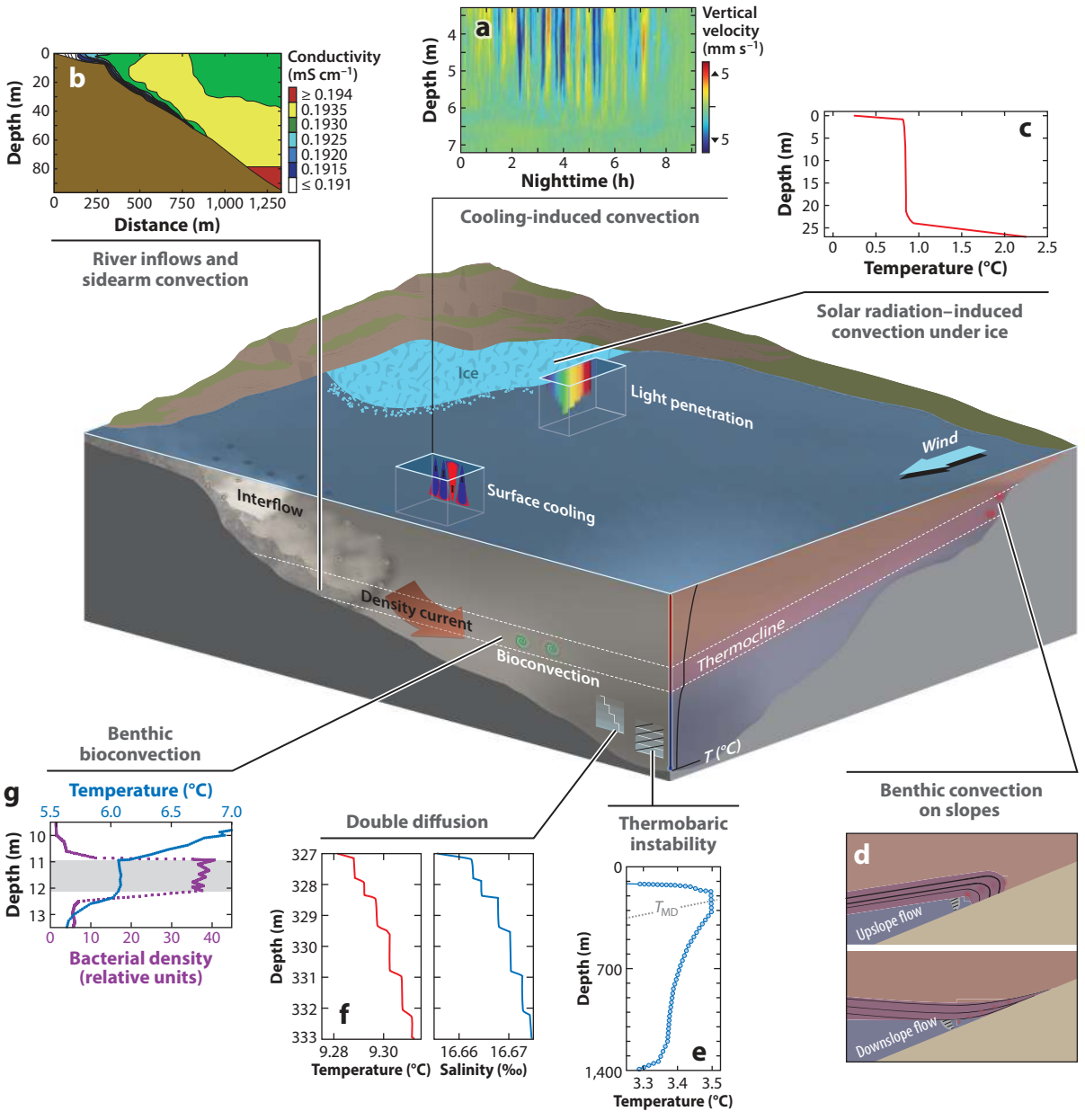

Figure 1

Schematics of the convective processes presented in this review: (*a*) cooling-induced convection at night (Section 2.1), (*b*) river inflows and sidearm convection (Sections 2.2 and 2.6), (*c*) solar radiation–induced convection under ice (Section 2.3), (*d*) benthic convection (Section 3), (*e*) thermobaric instability (Section 4), (*f*) double diffusion (Section 5), and (*g*) bioconvection (Section 6). Panels *a–g* adapted with permission from Jonas et al. (2003b), Fer et al. (2002), Bouffard et al. (2016), Davarpanah Jazi & Wells (2016), Wüest et al. (2005), Sommer et al. (2014), and Sommer et al. (2017), respectively.

other processes, through its effect on air–water gas exchange (Eugster et al. 2003, Rutgersson et al. 2011). Similarly, the skin-to-bulk parameterization of remotely sensed surface temperatures depends on the convectively driven surface turbulence (Emery et al. 2001, Wilson et al. 2013). The deepening of the convective mixed layer (CML) can also supply nutrients to the photic zone [i.e., on a daily timescale in tropical lakes (Verburg et al. 2003) or in fall and winter during deep convective mixing in higher-latitude lakes (Schwefel et al. 2016)].

An extensive review of the surface layer dynamics was done by Soloviev & Lukas (2014). We consider here the case for $\alpha > 0$ (i.e., $T > T_{MD}$; see the sidebar titled Density of Inland Waters) and negligible salt fluxes in freshwater. The surface heat flux H_{Q_0} is the sum $H_{Q_0} = H_{LW} + H_E + H_C$, where H_{LW} is the net longwave radiation, H_E is the latent (i.e., evaporation, precipitation) heat flux, and H_C is the sensible (i.e., conductive) heat flux (**Table 1**). Note that the shortwave solar radiation $H_{SW}(z)$ penetrates through the water column and therefore acts as a volumetric source of heat instead of a boundary flux. The radiation decreases according to specific depth-dependent attenuation coefficients that vary for each wavelength. In practice, the wavelength dependency is often integrated into an attenuation coefficient k_d (with units of inverse depth) of downwelling radiance measured by profiles of photosynthetically active radiation integrated over the range of 400–700 nm (as a synthetic proxy of monochromatic radiation in the visible range). From $H_{Q_0} > 0$ (upward heat flux) and $\alpha > 0$, the top of the water column becomes colder and denser than the water below and initiates gravitational Rayleigh-type instabilities. Yet, surface convection ($H_{Q_0} > 0$ at $\alpha > 0$) can also occur at times of net warming, and we have to account simultaneously for heating by solar radiation $H_{SW}(z)$ and cooling in the CML. The depth-varying heat flux is finally given by $H_Q(z) = H_{SW}(z) - \frac{z}{h_{CML}} H_{Q_0}$, in which $0 > z > -h_{CML}$ and h_{CML} represents the depth of CML.

We define an effective buoyancy flux B_* that represents the produced potential energy, which is available within the CML:

$$B_* = \frac{1}{h_{CML}} \int_{-h_{CML}}^{0} B(z)\mathrm{d}z = \frac{\alpha g}{\rho C_p h_{CML}} \int_{-h_{CML}}^{0} \frac{\partial H_Q(z)}{\partial z}(h_{CML} + z)\mathrm{d}z. \quad 3.$$

Note that we have $B_* = \frac{1}{2} B_0$ assuming a linear decrease of $B(z)$ for surface cooling at night. For daytime hours, it is useful to define a thermal compensation depth z_C, where $B(z)$ changes sign and where, at steady state, the opposite effects of heating and cooling compensate for each other: $k_d H_{SW}(z_C) = \frac{H_{Q_0}}{z_C}$. Assuming a case for which $H_{SW}(0) = -500$ W m^{-2} and $H_{Q_0} = 50$ W m^{-2} (i.e., a cold sunny day), z_C amounts to ~0.1 m in a turbid lake (for $k_d = 1$ m^{-1}) and ~0.5 m in a clear lake (for $k_d = 0.2$ m^{-1}). In reality, this layer is slightly deeper, as some heat is diffusing from below z_C, depending on the details of the temperature profile below z_C. We stress that surface convection occurs for all situations of $H_{Q_0} > 0$ and $\alpha > 0$, a condition that extends far beyond the classical nighttime cooling–induced convection.

From a phenomenology perspective, the thermal surface boundary forms a gravitationally unstable density difference. Yet, viscous/diffusive forces retard or prevent the onset of convective thermal plumes depending on the Rayleigh number (**Table 1**). The critical Rayleigh number [$\mathcal{O}(10^3)$] is already reached for a temperature difference of 0.1°C over a centimeter. For larger *Ra* [$\mathcal{O}(10^6)$], the convection is fully turbulent, which corresponds, for instance, to a temperature difference of 0.1°C over 1 m. At macroscale, we observe convective plumes descending as mushroom-like fluid parcels (Woods 2010) (**Figures 1*a*** and **2**). The convective scale velocity is given by $w_* = (B_* h_{CML})^{1/3}$ (Deardorff 1970). As the plumes impinge at the base of the convective layer, h_{CML} increases. The thermal plumes increase the temperature fluctuations at the top of the stratified layer underneath the CML that result from the transfer of kinetic energy of the plumes overshooting their equilibrium depth and radiating energy into the internal wave field (Townsend

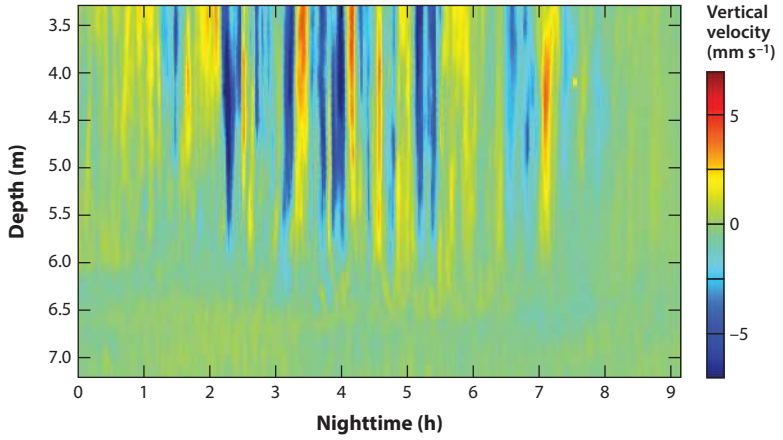

Figure 2

Cooling-induced penetrative convective mixing in the surface layer during nighttime hours as observed by vertical velocity measurements in a small lake. The heat map provides visualization of the thermal plumes between 3.3- and 7.2-m depth in the convective mixed layer (CML). Early in the night, we observe rapid deepening of the CML followed by almost stationary CML when the seasonal stratification with large N^2 is reached. Figure adapted with permission from Jonas et al. (2003b).

1964). This penetrative convection leads to a net entrainment and an expansion of h_{CML}. Deardorff (1970), Linden (1973), and Turner (1986), among others, suggested an initial deepening rate of h_{CML} scaling with $t^{0.5}$. Yet, the formation of a density jump between the convective region and the stratified layer below can limit the deepening rate of h_{CML} (i.e., lower power of t) (Linden 1975). A general expression is given by (Zilitinkevĭc 1991)

$$\frac{\mathrm{d}h_{\mathrm{CML}}}{\mathrm{d}t} = (1 + 2A)\,\frac{B_0}{h_{\mathrm{CML}} N^2}, \qquad 4.$$

where $N^2 = -\frac{g}{\rho}\frac{\partial \rho}{\partial z}$ is the background stratification immediately below the CML, and A is an entrainment coefficient (ranging between 0.1 and 0.3). From Equation 4, we directly infer that penetrative convection will speed up the mixed layer deepening compared to the nonpenetrative case by a factor of $(1 + 2A)$.

We continue with simplified ideal nighttime cooling (no solar radiation), shear-free homogeneous turbulence, and stationary turbulence in a CML, neglecting the penetrative convection. The turbulent kinetic energy (TKE) balance reduces in this case to buoyancy flux and dissipation (Wüest & Lorke 2003). When averaged over h_{CML}, the average dissipation $\bar{\varepsilon}$ of turbulent kinetic energy is proportional to, yet smaller than, B_*.

Yet, wind also contributes during the time of convection, especially in large lakes where wind shear stress ρu_*^2 almost never halts. The wind stress is estimated using $\rho_{\mathrm{a}}\, C_{10}\, W_{10}^2$, where W_{10} is the wind velocity measured at 10 m above the water surface, C_{10} is the drag coefficient, and ρ_{a} is the density of air. The Monin–Obukhov length scale, $L_{\mathrm{MO}} = u_*^3/kB_0$, where $k \approx 0.41$ is the von Kármán constant, defines the transition depth from shear-dominated turbulence at the surface to buoyancy-driven turbulence underneath ($B_0 > 0$). As an illustration, for a typical wind breeze of 2 m s^{-1} during a cold night, $H_{Q_0} = 50$ W m^{-2} leads to $L_{\mathrm{MO}} \approx -2$ m. The processes of wind stress and convection acting on the fluid column can be integrated using similarity scaling to estimate the depth distribution of turbulence as $\varepsilon(z) = c_1 \frac{u_*^3}{kz} + c_2 B_0$, with $c_1 \approx 0.6$ and $c_2 \approx 0.5$ empirically determined from measurements in lakes and the ocean (Shay & Gregg 1986, Jonas

et al. 2003b, Tedford et al. 2014). As pointed out by Tedford et al. (2014), a significant departure from the similarity scaling may indicate other active processes, such as erosion of the thermocline, restratification during the daytime due to solar radiation, or horizontal divergence in the TKE budget (Section 2.2).

There remain many open questions regarding near-surface convective dynamics relevant to other lake processes. Today, most skin-to-bulk parameterizations of the remotely sensed surface temperature do not include convection that affects the near-surface layer when $B_0 > 0$. Similarly, the recognition of inland waters as important emitters of greenhouse gases (Cole et al. 2007) requires more accurate implementations of the air–water gas exchange parameterization under convective low-wind conditions. Finally, heat and gas fluxes are affected by the presence of surfactants. This thin layer with dissolved organic matter is hardly ever taken into account. It is also important to link the convective turbulence to biogeochemical processes. Recent research on phytoplankton suggests that spring algal blooms depend on the level of turbulence in the photic zone (Peeters et al. 2007).

2.2. Differential Cooling

The classical thermal convection described in Section 2.1 becomes more complex in small lakes or lakes with dendritic-type shorelines (sidearms). Horizontal density gradients resulting from nearshore shallow water, cooling faster at night than offshore water, trigger a cross-shore transport (Farrow & Patterson 1993). This process, called differential cooling, was defined as a thermal siphon in a key pioneering study (Monismith et al. 1990). An example is the density current that was observed at night by Fer et al. (2002) in Lake Geneva (**Figures 1*b*** and **3**). The most common illustration of the basin-scale relevance of the thermal siphon is the role played by differential

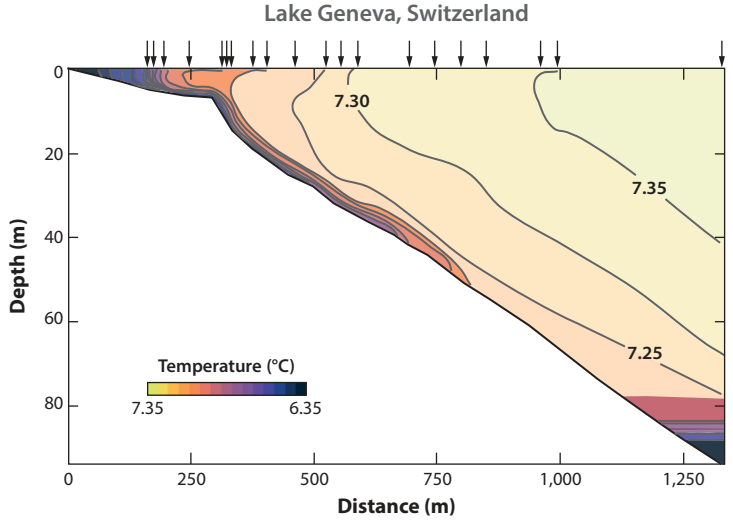

Figure 3

Isotherms derived from CTD (conductivity, temperature, depth) profiling (*top arrows*) indicate a nearshore transect of Lake Geneva, showing a density current induced by sidearm cooling flowing downslope. If scaled up, based on observed mass transport, buoyancy flux, and lake bathymetry, this process would lead to a downward cross-shore transport of 11 times that of the main tributary (Rhône River) during winter. Figure adapted with permission from Fer et al. (2002).

cooling for wintertime deep mixing. Peeters et al. (2003) suggested that the cold, deep water at the bottom of 668-m-deep Lake Issyk-Kul originated from this differential cooling. Another example is Lake Tanganyika, where differential cooling was found to be the main driver of the 600-km basin-scale circulation (Verburg et al. 2011), which is conceptually similar to the global ocean overturning circulation.

The concept of differential cooling leads to two main questions: What is the relevance of differential cooling for (*a*) the flushing or retention time of nearshore water and (*b*) the fate of the cross-shore transport affecting the deep water quality? From laboratory experiments using a reservoir with a triangular setting (e.g., with a bottom slope $s = \tan\theta$ and a horizontal length L) and from scaling analysis, Sturman et al. (1999) described the discharge rate per unit length of shoreline, Q ($m^2\ s^{-1}$), and the shore volume flushing time, τ, under steady-state conditions as follows:

$$Q = 0.24 {B_*}^{1/3} \left(\frac{L \tan\theta}{1 + \tan\theta} \right)^{4/3} \quad \text{and} \quad \tau \sim L^{2/3} \frac{(1 + \tan\theta)^{4/3}}{(B_* \tan\theta)^{1/3}}. \qquad 5.$$

Lei & Patterson (2005) proposed a scaling for the onset of instability in the wedge-shaped region and suggested differentiation into three regions: a nearshore, conduction-dominated region (nearly vertical isotherms); an intermediate, stable, convection-dominated region (heat transfer dominated by bottom-following density currents); and an offshore, unstable, convection-dominated region (heat transfer dominated by sinking/rising plumes). Mao et al. (2010) used a two-dimensional wedge model to express the cross-shore extent of these three regions based on the wedge shape ratio and *Ra*.

Much of what is known about the transport induced by sidearm differential cooling comes from studies of river underflows (Alavian et al. 1992, Hogg et al. 2013, Cortés et al. 2014). There, the flow path is split into three dynamically different regimes, starting with a plunging stage, followed by an underflow stage, and finally an intrusion stage. Ellison & Turner (1959) were the first to apply the governing integral equation for two-dimensional gravity currents over a slope. They suggested that the entrainment is proportional to the propagating speed of the gravity current and to an entrainment coefficient E (**Table 1**) (Parker et al. 1987, Cenedese & Adduce 2010, Wells et al. 2010). Such an entrainment model allows one to predict the properties of the downstream evolution of the density current. The main differences between river underflows and sidearm differential cooling are due to the initial conditions. In the riverine case, the intruding water has a limited area, a large momentum, and a nearly continuous flow, while in the sidearm case, the area is much larger, with an initially weak momentum (e.g., no plunge stage) and a daily varying timescale.

The fate of the density current depends not only on the properties of the currents and the slope but also on the local lake density profile. Wells & Nadarajah (2009) proposed a scaling for the intrusion depth Z_{eq} as a function of the background linear stratification N^2 and B_*. Yet, multiple intrusions into a background homogeneous stratification are also possible as a result of density gradients within the plume. These gradients result from a partial mixing of the entrained ambient fluid into the density current (Baines 2001). This process is known as detrainment.

Most research on density currents is laboratory based. Thus, there are questions regarding how realistic the results are after scaling up to real-world lake dimensions. From a lake ecosystem perspective, lakes must be connected to their lateral boundaries, and the horizontal transport of nutrients, gases, pollutants, and the like from the littoral into the pelagic zone needs to be quantified, notably the role of differential cooling. Simple asymptotic models have been developed, but they should be refined by integrating the interaction of the sidearm cooling with other lake processes.

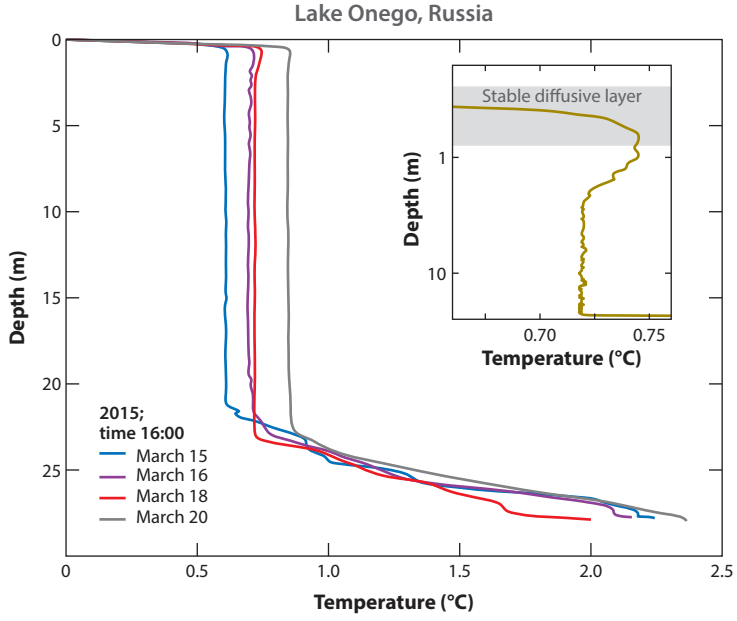

Figure 4

Temperature profiles in Lake Onego (Russia) taken at 16:00 (local time) on March 15, 16, 18, and 20, 2015. These profiles show the thermal structure of the radiatively driven convection as well as the layers deepening and increasing the background potential energy. (*Inset*) The under-ice diffusive boundary layer (log scale). Figure adapted with permission from Bouffard et al. (2016).

2.3. Under-Ice Radiation

One of the most remarkable types of convection occurs under the ice cover in late winter (**Figure 1*c***). Ice-covered lakes are characterized by surface water temperatures below T_{MD} ($\alpha < 0$) (**Table 1**) and protected from wind stress. In late winter, as soon as snow disappears from the ice surface, the volumetric radiative warming (Section 2.1) deposits heat into the upper layer, leading to gravitational instability and convection (Farmer 1975, Matthews & Heaney 1987). Due to the weak solar radiation, the resulting buoyancy flux and convectively driven mixing are also weak. Thus, it is no surprise that under-ice biogeochemical and physical processes have been long ignored for inland waters (Kirillin et al. 2012, Powers & Hampton 2016), and studies of radiatively driven convection in ice-covered lakes are rare (Mortimer & Mackereth 1958, Farmer 1975, Mironov et al. 2002, Jonas et al. 2003a).

The radiatively driven under-ice convection differs from the classical one described in Section 2.1 in that (*a*) the forcing is now a volume source, in contrast to the surface cooling, and (*b*) the CML is separated from the ice by a thin, stable diffusive layer of thickness δ (**Figure 4**), which modifies the upper limit of the CML in Equation 3. Yet, as in Section 2.1, the CML is characterized by the thermal plume velocities and the subsequent deepening of the CML, both of which are dependent on solar radiation and on the light absorption. In situ observations typically reported $w_* \approx 1$–7 mm s^{-1} (Bouffard et al. 2016) and CML-deepening rates of ∼0.5 m day^{-1} reaching up to 3 m day^{-1} for strong solar radiation and weak background stratification (Kirillin et al. 2012).

Similar to the case $\alpha > 0$, differential heating between the littoral and pelagic zone can lead to large-scale circulation, as shown by the lake-wide anticyclonic gyres described by Kirillin et al.

(2015) and Forrest et al. (2013). The forcing, which leads to nearshore density currents, is a combination of the differential warming from solar radiation and the release of heat from the sediments that accumulated during the previous ice-free period.

The absence of wind-induced shear below the ice cover makes the underlying lake an ideal natural laboratory for studying radiatively driven convection. Questions to be addressed concern the energy partitioning between dissipation and the increase in background potential energy, as well as the mixing efficiency of radiatively driven convection (Ulloa et al. 2018). While the mixing efficiency is typically ∼0.2 for shear-driven turbulence (Peltier & Caulfield 2003, Ivey et al. 2008, Gregg et al. 2018), it can reach 0.5 for Rayleigh–Bénard convection (Hughes et al. 2013). Further challenges are the parameterizations of the heat transfer through the ice and the wavelength- and depth-dependent heat absorption below the ice. Modern autonomous underwater vehicles provide tools to study the fascinating structures observed in radiatively driven convection, such as the intriguing ice holes on Lake Baikal (Kouraev et al. 2016). Under-ice convection has been found to trigger early growth of phytoplankton (Vehmaa & Salonen 2009), as the convective thermals mix nutrients close to the ice and keep nonmotile phytoplankton in the photic layer (Kelley 1997).

2.4. Sediment–Water Heat Fluxes

So far, we have discussed cooling-induced convection initiated at the surface (Sections 2.1 and 2.2) and the volumetric radiation-induced convection in the layer under ice (Section 2.3). However, heat fluxes at the sediment–water interfaces also generate buoyancy flux and convective mixing right above the sediment. Transient or permanent convective mixing will tend to homogenize the bottom boundary layer (BBL) and eventually the lake circulation (Section 2.3), and it will partly influence the ecosystem functioning via nutrients and gas transport.

The radioactivity in Earth's interior generates an average geothermal flux of ∼0.065 W m^{-2} over the continental crust. Depending on the dynamics of Earth's mantle, local fluxes deviate largely, attaining values of ∼0.1 W m^{-2} in active Central (Alpine) Europe (Finckh 1981) or very large values in volcanic regions (Boehrer et al. 2009b). These fluxes remain mostly small compared to typical atmospheric or riverine heat input and they are thus often neglected. However, accurately measured temperatures in deep lakes often reveal an increase above the sediment during undisturbed periods between deep convective mixing events. Tivey et al. (2016) reported a daily deep water temperature increase of ∼1 mK in the geothermally active Lake Rotomahana, resulting from an average sediment heat flux of 21 W m^{-2}.

Pore water convection in the top sediment layer is another source of heat input to the BBL. It results from gravitational instabilities when colder water overlays the warmer sediment. This scenario is found at daily-to-seasonal timescales. In shallow waters, where solar radiation penetrates to the bottom, the sediments are warmed. At night, the sediment surface acts as a heat source and releases the daily accumulated heat to the overlaying colder water. Similarly, upwelling resulting from basin-scale internal waves (such as seiches) triggers local gravitational instabilities in the colder, upward-moving layers. Kirillin et al. (2009) showed that internal wave periods of 0.5 h or longer could sustain cold water on top of warm sediments long enough to trigger pore water convection within the sediment. At longer seasonal timescales, deep cooling-induced convective mixing in winter (Fang & Stefan 1996) can also lead to gravitational instabilities above the warmer sediment. The subsequent sediment–water heat fluxes have been shown to modulate the nutrient concentrations in the BBL (Golosov & Ignatieva 1999).

A current challenge is to simultaneously model these two types of sediment–water heat fluxes in combination with shear-induced convection (Section 3) for biogeochemically relevant applications.

2.5. Evaporation in Salty Lakes

So far, we have used the thermal contribution only to quantify the buoyancy flux in Equation 1. This simplification is valid most of the time for freshwater lakes. However, in salty lakes, surface convection can also be driven by the downward salt flux, $H_{S_0} = \frac{S}{L_E(1-S)} H_E$ (kg m^{-2} s^{-1}), which results from the latent heat flux H_E (W m^{-2}) of evaporation of water with salinity S and where L_E (J g^{-1}) is the latent heat of water. One of the most spectacular examples of convection driven by changes in salt concentration is the historical overturn of the hypersaline Dead Sea in 1979, which changed the lake from meromictic (i.e., a lake with a permanent stratification, often resulting from a strong salinity gradient) to holomictic (i.e., a lake with at least one complete mixing—destratification—per year) (Steinhorn 1985, Anati et al. 1987). The most obvious reason was the decrease in freshwater input from the Jordan River during dry seasons such that it no longer balanced the surface salt increase by evaporation. The excess salt finally removed the density contrast between the surface and deep water and substantially increased the surface buoyancy flux B_0 (Equation 2) responsible for present-day deep mixing that recurs during cooler periods.

Another salinity-driven convective process is observed during the freezing process in saline ice-covered lakes such as pit lakes. The salt exclusion during ice formation leads to a downward salt flux (Pieters & Lawrence 2009) identical to evaporation as described above.

2.6. River Inflows

The last boundaries of lakes to be considered are the river inflows. The underflow dynamics are described in detail in Legg (2012) and summarized in Section 2.2. We focus here on other river-induced sources of convection. The first process paradoxically concerns lighter-density river water that can lead to underflow when the river temperature is warmer (cooler) than T_{MD} while the lake temperature is cooler (warmer) than T_{MD}. The river inflow mixes at the surface with lake water and the mixture of the two waters contains water of temperature T_{MD} that is denser than the two original waters and will therefore sink along the slope as a density current. This cabbeling effect was reported by Rodgers (1965) and Carmack et al. (1979) and has since been observed in many lakes in cold regions.

The second process involves the high concentration of particles in a warm riverine inflow. So-called particle-laden flows can lead to double-diffusive fingering (Section 5) below the warm riverine intrusion (Davarpanah Jazi & Wells 2016). Once the particle-laden water has intruded into the interior of the receiving water body, the suspended sediment particles will settle out and the riverine water (without particles) may become lighter and cause convective plumes (Sutherland et al. 2018).

Lakes are now recognized as integrating sentinels of the watershed responding to anthropogenic changes (Adrian et al. 2009). Rivers typically provide nutrients, organic and inorganic particles, and dissolved oxygen at depths where the inflow equilibrates in density with the ambient lake water (Bouffard & Perga 2016, Fink et al. 2016, Råman Vinnå et al. 2018). Hence, the dynamics of buoyancy-driven flows over a sloping boundary remains key for understanding cross-shore exchanges and their relevance for the ecosystem.

3. SHEAR-INDUCED CONVECTION OVER SLOPES

The original observations of this type of convective mixing were made in open estuaries. We consider seaward-floating freshwater on top of heavier ocean water, thereby forming strong density stratification. During tidal flooding, ocean water is driven into the estuary, where it reduces the

stratification, whereas the opposing ebb strongly stratifies the freshwater-influenced estuary. This phenomenon, often called tidal straining (Simpson et al. 1990), leads to a distinct semidiurnal variation in stratification with almost complete vertical mixing in high waters. Taking microstructure measurements in the freshwater-influenced Liverpool Bay, Rippeth et al. (2001) found strong dissipation during the ebb only in the lower stratified water, whereas during tidal flooding, the eroded stratification allowed vertical mixing with density instabilities and convective mixing throughout the water column. Although not observed in lakes, this phenomenon of periodic straining and stratification reveals that the mechanism of convective turbulence is also important in lakes.

The setting for this process is illustrated in the BBL shown in **Figure 1*d***. In stratified lakes, winds excite omnipresent basin-scale internal seiches (Imberger 1998). The subsequent periodic bidirectional flow leads to alternating shear above the lake bed. As indicated in **Figure 1*d***, the effect of the back-and-forth flow of the stratified layers causes a periodic variation in the stratification of the sloped BBL. During the upslope flow phase, the layer directly above the sediment moves slowly (no slip at sediment) compared to water some distance above the sediment (**Figure 1*d***). Hence, the more distant water travels a longer distance parallel to the tilted lake bed compared to near-sediment water (differential advection). Given the background stratification, the denser water parcels from greater depth end up on top of the shallower and lighter water and cause instabilities, as exemplified in **Figure 5** (Lorke et al. 2005). During the opposite downslope flows

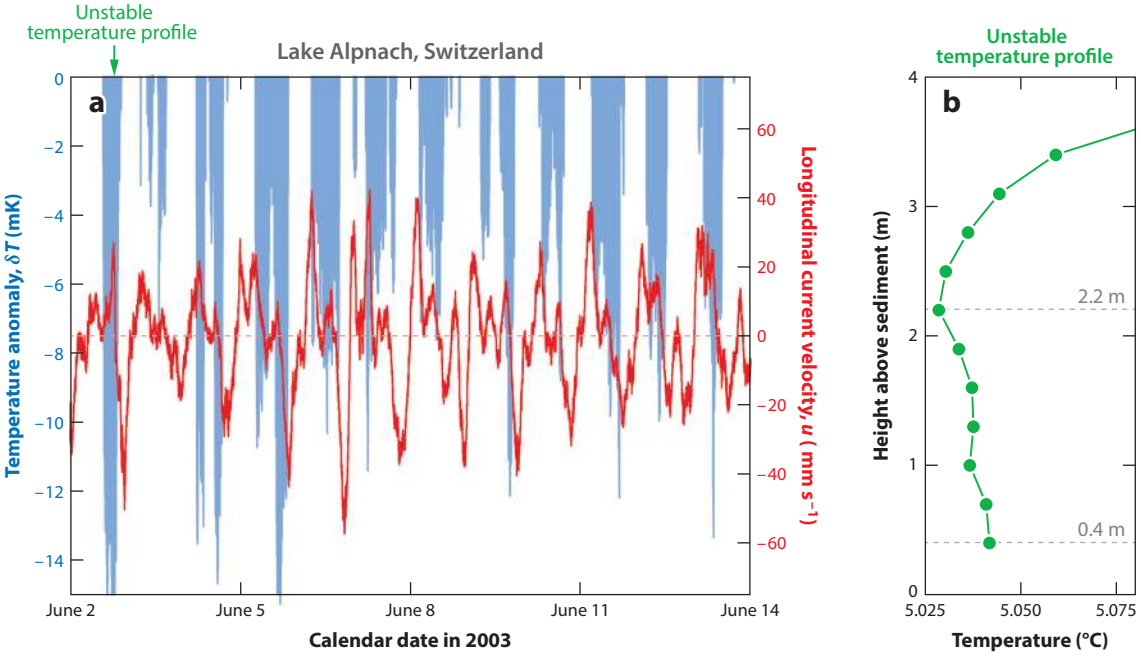

Figure 5

Shear-induced convection above a lake bed with slope of ∼0.006 and a parallel-slope temperature gradient $\partial T/\partial x = 0.1°C/250$ m. Together with the convective layer height $h = 2.5$ m, the maximum current velocity of the seiching $u = 3$ cm s^{-1} and the thermal expansivity $\alpha = 24 \times 10^{-6}$ °C^{-1} (for 5.5°C water; **Table 1**) result in an upper bound of the buoyancy flux $B(h) \approx 7 \times 10^{-9}$ W kg^{-1}, as confirmed by dissipation measurements (Lorke et al. 2005). (*a*) A twelve-day time series of the along-lake current velocity u (*red line*, *right scale*) and temperature anomaly δT (*light-blue shading*, *left scale*) in the bottom boundary layer (BBL) of Lake Alpnach at 31-m depth. The anomaly δT is the temperature difference between 2.2 and 0.4 m above the sediment (*dashed lines* in panel *b*). Positive upslope currents lead to negative δT (*blue shading*), causing unstable stratification (positive δT with stable BBL not shown). (*b*) An example of an unstable temperature profile (time indicated by the *green arrow* in panel *a*). Figure adapted with permission from Lorke et al. (2005).

half a seiche period later, shallow, lighter water moves on top of heavier water (**Figure 1*d***), which results in enhanced stratification directly above the sediment (**Figure 5**).

An observation of seiches within parallel-slope temperature gradients is documented in **Figure 5**. Analogous to boundary-induced convection (Section 2), the level of turbulence can be characterized as a function of height h above the sediment by the buoyancy flux $B(h)$, which is defined by the covariance of the vertical velocity w' and density ρ' fluctuations (Equation 1) and can be quantified by ($\partial\rho = -\rho\alpha\ \partial T$)

$$B(h) = -\frac{g}{\rho}\overline{\rho' w'} \approx \frac{g}{\rho} h \frac{\partial \rho}{\partial t} = g\alpha h \frac{\partial T}{\partial t} = g\alpha h u \frac{\partial T}{\partial x}. \quad 6.$$

For this approximation, it is assumed that the downward density flux leads to a homogeneous density increase over the CML of thickness h in the BBL. Equation 6 is consistent with our expectations that shear-induced convective turbulence increases with α, current u, thickness h, and the along-slope temperature gradient $\partial T/\partial x$ (see values in **Figure 5**). The practical implications are that strongly excited basin-scale seiching (u) causes a thicker BBL with stronger convective turbulence. In Lake Ontario, seiche-induced vertical thermocline deflections of up to 15 m have been observed, which resulted in diffusivities varying by a factor of 500. This occurred synchronously to the remarkable asymmetry in near-bed stratification, which oscillated between instability and $\sim$1 K m^{-1} (Chowdhury et al. 2016). Although the details differ with the depth, slope, temperature (larger α for warmer water), and type of basin-scale waves, the common asymmetry in BBL stratification and turbulence is directly related to upslope and downslope flows, as shown in situ (Lorke et al. 2008, Cossu & Wells 2013) and for models (Becherer & Umlauf 2011, Lorrai et al. 2011). Unsurprisingly, BBL convection was first identified on the continental shelf (Moum et al. 2004), where ocean currents u (tides) are much larger than in lakes.

Given that all lake beds are sloped and seiching in enclosed waters is almost omnipresent, one may wonder why this phenomenon has been overlooked for so long. However, a high-temperature resolution of $\sim$1 mK (**Figure 5**) was not routinely available on most limnological CTD (conductivity, temperature, depth) instruments. It is still not fully clarified what shear-induced BBL convection contributes to the overall mixing in stratified deep water. Model results indicate that convective turbulence during upflow inefficiently mixes already homogenized BBL water. During the strongly stratified downflow phase, BBL turbulence is suppressed (Chowdhury et al. 2016). Hence, the question remains how efficiently the BBL water exchanges with interior water to store the potential energy generated by BBL turbulence (Becherer & Umlauf 2011, Lorrai et al. 2011). It is probable that more intense shear-induced convection forms thicker homogenized BBLs with larger density differences compared to the interior water, leading to stronger gravitational forces and more lateral exchange. Convective BBL mixing has biogeochemical implications in and above the sediment, as oxygen is brought close to the sediment and redissolved solutes (nutrients) are removed from the sediment surface. As an overall effect, the exchange of biogeochemical constituents between the stratified interior and the BBL is intensified (Henderson 2016).

4. THERMOBARIC CONVECTION IN DEEP LAKES

4.1. Effect of Pressure on Permanent Stratification in Cold, Deep Lakes

Deep water renewal in freshwater lakes occurs during ice-free winter periods (temperate regions) and during dry seasons (tropics). Such renewals regularly remove potentially stagnant, low-oxygen deep water on a seasonal scale. Therefore, the extent to which water bodies experience convection to maximum depth (holomixis) is an intrinsic ecological concern. Lakes with several 100-m-deep

volumes often reveal permanent winter stratification, even when water is coldest at the surface. Examples are Quesnel Lake (Laval et al. 2008, 2012), Crater Lake (Crawford & Collier 1997, 2007), Lake Shikotsu (Boehrer et al. 2009b), Lake Baikal (Carmack & Weiss 1991), and several deep lakes in Norway (Boehrer et al. 2013). If there are no water constituents affecting the density (salinity $\approx$ 0 ‰), the peculiar freshwater pressure dependency of the equation of state (see the sidebar titled Density of Inland Waters) is responsible for such permanent deep water stratification (Chen & Millero 1986, Boehrer & Schultze 2008), as explained below.

At the surface of low-salinity waters, the density reaches its maximum at $T_{MD} \approx 4$°C. With increasing depth/pressure, T_{MD} decreases (see the sidebar titled Density of Inland Waters). For waters deeper than ~2,900 m, freezing would occur before T_{MD} is reached. With a depth of 1,637 m, Lake Baikal is however the deepest lake and therefore this phenomenon is only known for lakes frozen into deep ice in Antarctica, such as Lake Vostok (Wüest & Carmack 2000). During the warm season with classical stratification $T > T_{MD}$ (i.e., $\alpha > 0$), gradients $\partial T/\partial z$ are positive upward and lake water columns are stably stratified (common in temperate lakes). During the cold season, the surface cools below T_{MD} (**Figures 1*e*** and **6**) and $\alpha < 0$. For this setting, we conclude that the water column is stable everywhere as long as the transition from the surface layer (α and $\partial T/\partial z$ both negative) to the deep layer (α and $\partial T/\partial z$ both positive) occurs at exactly the depth where α and $\partial T/\partial z$ both pass through zero, implying $T = T_{MD}$ ($\alpha = 0$). In the T profile shown in **Figure 6**, this is the case at ~230-m depth, where $\partial T/\partial z = 0$ and T reaches its maximum (T_{MD} line). This can be generalized so that, for a stable water column in winter, when surface T is less than T_{MD}, the T profile reaches a maximum—often called the mesothermal maximum—at

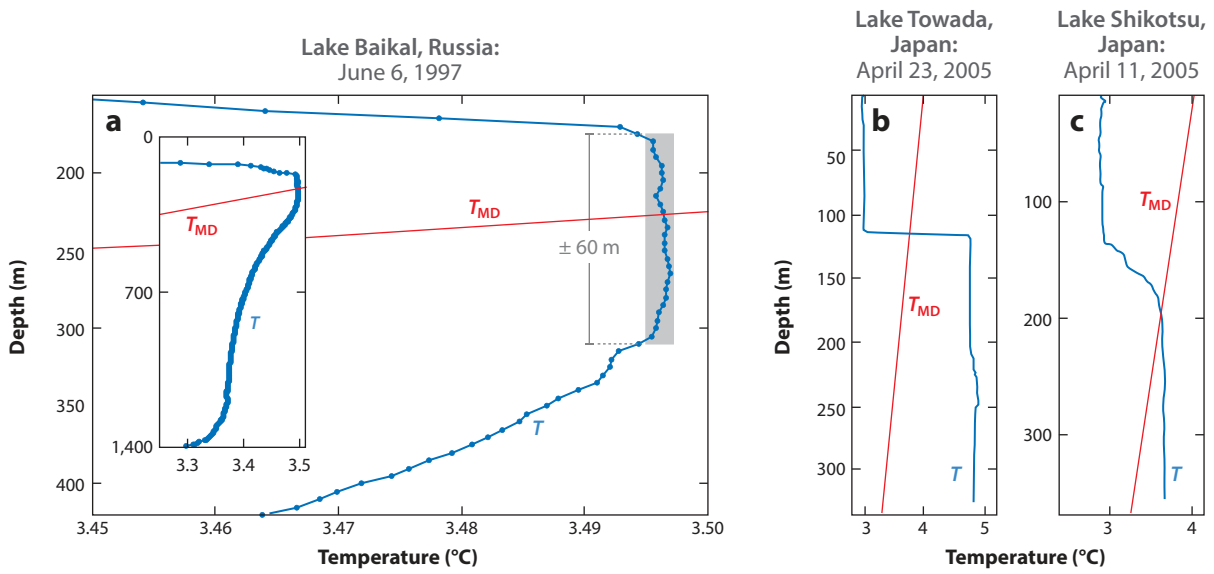

Figure 6

Thermobaric instability at the mesothermal maximum of deep lakes. (*a*) Temperature (T) profile in Lake Baikal on June 6, 1997, indicating the cold and inversely stratified surface layer (above 200-m depth), the permanently stratified deep water (below 300-m depth), and the homogenized layer where the mesothermal temperature maximum crosses the line of temperature of maximum density, T_{MD}. The uniformity at 230 $\pm$ 60 m is a result of thermobaric convective mixing. (*Inset*) Depiction of the entire T profile. (*b*) T profile from April 23, 2005, in Lake Towada, where T crosses $T_{MD} = 3.8$°C at ~110-m depth. (*c*) T profile from April 11, 2005, in Lake Shikotsu with the corresponding crossover at 3.6°C at ~200-m depth. Panel *a* is adapted with permission from Wüest et al. (2005) and panels *b* and *c* from Boehrer et al. (2009b).

the depth where $T = T_{MD}$. **Figure 6** shows two examples in addition to Lake Baikal, documenting that many other deep lakes show the same crossovers.

4.2. Thermobaric Instability and Convection

The phenomenon of thermobaric convection is evidently recognizable in the Lake Baikal temperature profile right after ice breakup, and it reveals an impressive homogeneous layer approximately 130 m thick (**Figure 6**) that formed during the preceding period under ice. Any vertical displacement of the mesothermal maximum away from the T_{MD} line leads locally to so-called thermobaric instabilities due to the pressure dependence of α. When a baroclinic deflection (as by internal waves) shifts the water column upward, the mesothermal maximum is above the T_{MD} line and no longer aligned to T_{MD}. Consequently, the layer between the mesothermal maximum and T_{MD} keeps its positive $\partial T/\partial z$ gradient, whereas α turns negative and therefore becomes unstable ($N^2 < 0$). The symmetrical case of baroclinic downward movement would lead exactly to an identical instability between the T_{MD} line and the mesothermal maximum below. This analysis demonstrates that the water masses between the mesothermal maximum and the T_{MD} line are always unstable and cause weak convective turbulence whenever baroclinic activities are present under ice. Therefore, the mesothermal maximum is not a well-defined maximum but is rather a mixed layer of almost homogeneous temperature (**Figure 6**).

From the T profile relative to the T_{MD} line in **Figure 6**, it is evident that the vertical deflections during the preceding period of ice cover were at least ± 60 m. However, from the profile we cannot gain any indication on the temporal or length distribution of those internal deflections during the previous winter. Here, forcing is very different from cooling- or radiation-induced convection (Sections 2.1 and 2.3). In the center of the mixed layer, T equals T_{MD} ($\alpha = 0$) and the buoyancy flux $B(z)$ (Equation 1) vanishes, whereas it is largest at both the upper and lower boundaries of the homogeneous layer. The influence of this unusual structure of $B(z)$ on the convective turbulence has never been investigated in lakes.

In addition to the thickness of the homogeneous layer, the depth level at the end of the winter is an indicator of the activity under ice. With increasing turbulence above the mesothermal maximum (i.e., in the region of $\alpha < 0$), more heat is transported upward. As a result, the mesothermal maximum erodes faster and therefore the mesothermal front moves downward. Conversely, if the water is quiet, as in a small wind-protected lake, the heat removal is slow and the mesothermal maximum stays shallow.

An important practical question is how the permanently stratified deep water below the mesothermal maximum is renewed, as the classic seasonal deep convective mixing is absent. However, as most of these lakes show high oxygen levels, despite their continuous stratification (Boehrer et al. 2013, Gulati et al. 2017), this indicates that deep water renewal is efficient enough to prevent the formation of biogeochemical gradients. One answer can be found in the observations of Schmid et al. (2008), which revealed that a long-lasting wind pushed the cold surface water to a depth at which α turned positive and the forced surface water could freely sink to the deepest zones.

5. DOUBLE-DIFFUSIVE CONVECTION

Double diffusion (DD) has been found in various geophysical settings and even occurs within stars (Garaud 2018; see the sidebar titled Past Double-Diffusive Research). In lakes, DD plays a role in two different ways, which are explained in the following. Active DD convection in stratified waters is usually conjectured when well-defined quasi-homogeneous horizontal layers are

PAST DOUBLE-DIFFUSIVE RESEARCH

The phenomenon of differential diffusion (DD) with very dissimilar molecular diffusivities has been long known in medical and chemical research. However, the potential of DD as a driver of environmental flows in natural waters was only recognized in the late 1950s by Stommel et al. (1956) and Stern (1960) based on theoretical considerations and laboratory experiments (Turner 1974). The diffusive type of DD was thoroughly studied in the 1970s when artificially stratified solar ponds (Weinberger 1964) were investigated for renewable heat recovery (Velmurugan & Srithar 2008). The first discovery of a DD staircase in lakes was in the ice-covered and permanently stratified Lake Vanda in the Dry Valley of Antarctica (Hoare 1966). Meanwhile, both regimes of DD (fingering and diffusive-type) have been observed in various lakes worldwide when their stratifications were favored by the biogeochemical, geological, and hydrological environments (Wüest et al. 2012). Here, we do not consider the more common oceanic thermohaline staircases, which are found in the relatively quiescent tropical and subtropical thermoclines (Schmitt 1994) and the high-latitude Arctic oceans (Shibley et al. 2017).

observed. These layers are separated by thin and strongly stratified interfaces in overall stable water columns (**Figure 1*f***). Still, it remains poorly understood what initiates this specific form of convection that leads to layering (**Figure 7*a***) over large vertical and horizontal regions. DD convection occurs when three conditions are fulfilled: (*a*) The vertical density profile must depend on at least two constituents with opposing contributions to stability N^2 (one stabilizing, one destabilizing). (*b*) These two contributions to the overall stability $N^2 > 0$ are of similar absolute magnitude. (*c*) The two constituents have substantially different molecular diffusivities (e.g., $D_T \approx 1.4 \times 10^{-7}$ and $D_S \approx 2 \times 10^{-9}$ m^2 s^{-1} for temperature and dissolved substances, respectively). We show below that weak background turbulence is usually also a requirement for DD to become

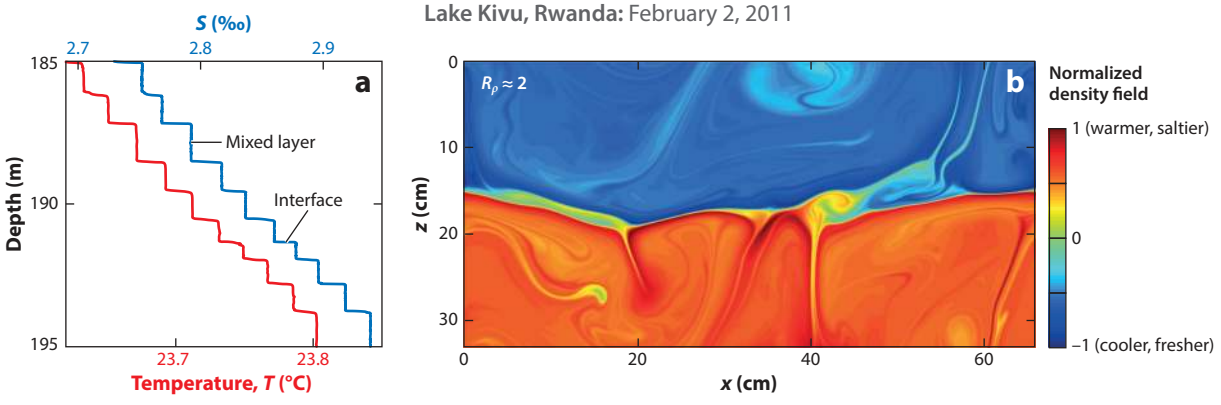

Figure 7

Double-diffusive convection in Lake Kivu. (*a*) A 10-m-long profile section of a double-diffusive temperature (*red*) staircase and salinity (*blue*) staircase from February 2, 2011. Typical scales of the interfaces are thicknesses of ~6 and ~9 cm for salinity and temperature, respectively, and ~70 cm for the height of the well-mixed layers (for further detail, see Sommer et al. 2013). (*b*) Convective structures generated by direct numerical simulation for a diffusive-type of double diffusion of a Lake Kivu interface with adjacent mixed layers for $R_\rho \approx 2$ and realistic background stratification as in panel *a*. The colors represent the density field (normalized with respect to the mean density and the maximum density difference), with blue for cooler and fresher water versus red for warmer and saltier water. Figure adapted with permission from Sommer et al. (2014).

dominant. The faster-diffusing constituent (temperature) generates local instabilities in the overall stable density profile, and the produced buoyancy flux drives the DD convection. The physical setting is framed by two stratification parameters: the water column stability N^2 and the density ratio R_ρ (Garaud 2018; **Table 1**), which is the nondimensional ratio of the positive contribution divided by the negative contribution to N^2. Layering is usually found if the range of R_ρ is $1.5 < R_\rho < 6$, although DD-favorable conditions exist theoretically over the much wider range of $1 < R_\rho < D_T/D_S$.

We occasionally find (bio-)geochemical environments in lakes, where additional constituents stabilize or destabilize the density profiles. Examples of triple diffusion are Lake Nyos (Schmid et al. 2004a) and Lake Banyoles (Sánchez & Roget 2007), where salinity/carbon dioxide and salinity/particles stabilize the water column, respectively. Finally, we discuss below the water column of Lake Kivu, which has two stabilizing components (salinity and carbon dioxide) and two destabilizing components (temperature and methane), representing the most prominent example of quadruple diffusion. We distinguish between fingering convection, where temperature (stabilizing) and salinity both decrease with depth (e.g., Dead Sea), and oscillatory DD convection, where salinity (stabilizing) and temperature both increase with depth (e.g., Lake Kivu in **Figure 7*a***).

5.1. Double-Diffusive Favoring Environments

The finger regime is rarely reported for inland waters and is probably restricted to salty lakes. In the Dead Sea, fingering occurs in the upper thermocline at times of strong seasonal solar influx (Section 2.4), subsequent high surface temperatures, and high evaporation-induced salinity (Anati & Stiller 1991). However, much more frequent is the diffusive regime due to various geophysical and biogeochemical settings that provide the deep subaquatic sources for temperature and salinity.

Permanent diffusive-type stratification is found in several coastal ex-fjord lakes on the northwest coasts of Europe and Canada, where ancient seawater resides beneath freshwater. Examples are the 92-m-deep Norwegian Rørhopvatn (Strøm 1962) or the ∼340-m-deep Powell Lake (British Columbia), which contain trapped seawater at great depth. As a result of the glacio-isostatic rebound, the fjords were lifted and separated from the ocean and formed inland lakes. Over the past 11,500 years, geothermal heat in Powell Lake warmed the ∼17 ‰ salinity deep water up to 9.4°C (Scheifele et al. 2014). Similarly, ice-covered lakes in Antarctica are also double-diffusively stratified by salt brines originating from ancient evaporation. Overflowing light freshwater causes high-stability N^2, which suppresses diffusion down to the molecular level. A fascinating phenomenon occurs in Lake Vanda, where despite the ice cover, sunlight penetrates into the underlying water and warms the stratified water column (Section 2.3) so that it reaches cozy temperatures of ∼25°C in the deepest layers, despite the extremely low average polar air temperatures of −17°C (Wilson & Wellman 1962, Huppert & Turner 1972).

Heat and salt input, required for a diffusive type of DD, can enter directly by subaquatic springs, as in Lake Nyos (Schmid et al. 2004a) and Lake Kivu (Newman 1976, Schmid et al. 2010, Sommer et al. 2013). Besides deep geothermal sources, lakes are also exposed to shallow-type subaquatic springs, which are fed by ground- and rainwater and are often related to higher temperature and particle inputs (Sánchez & Roget 2007). Stratification favorable to DD convection is also found in iron-meromictic (pit) lakes, where groundwater carries dissolved iron from tailings into the anoxic deep water (Boehrer et al. 2009a). As iron precipitates in the oxic surface layer, a strong gradient of dissolved iron is maintained, which stabilizes the density profile against temperature and creates a seasonal DD staircase (Von Rohden et al. 2010).

5.2. Double-Diffusive Layering in Lakes

There are various explanations for DD convection. As molecular heat diffusion ($\sim 1.4 \times 10^{-7}$ m^2 s^{-1}) is ~100 times faster than molecular salt diffusion ($\sim 2 \times 10^{-9}$ m^2 s^{-1}), the transition zone between the stable interface and the two adjacent well-mixed layers (**Figure 7*a***) experiences diffusion-induced changes in temperature but hardly any changes in salinity. As shown graphically in figure 1 of Carpenter et al. (2012b), molecular diffusion leads to broadening of the T interface, and subsequently, this thin transition zone between interface and mixed layer becomes unstable. These instabilities drive in the layers above and below the thermals away from the interfaces (**Figure 7*b***), thereby maintaining quasi-homogeneous layers and steep interface gradients (Huppert & Linden 1979).

Typical interface steps of temperature and salinity are $\Delta T \approx 10$ mK and $\Delta S \approx 0.013$ ‰, with an average interface thicknesses of ~6 and ~9 cm for salinity and temperature, respectively, and average mixed layer heights of ~70 cm (**Figure 7*a***). Although these values were observed in Lake Kivu (Sommer et al. 2013), they are also representative of other lakes (Toffolon et al. 2015) and even the Arctic ocean (Timmermans et al. 2008) and can be considered typical for lakes. Idealized direct numerical simulations (DNS) by Carpenter et al. (2012a), together with such observations, prove that the vertical fluxes of heat and salt through the core of the interface have a purely molecular nature.

The detailed vertical structure of the DD layering gives rise to various questions concerning the number of layers, the interface steps, and the thicknesses of the layers and interfaces. Interestingly, Toffolon et al. (2015) showed that for observed stability N^2 and density ratios R_ρ, the number of layers and their dimensions could be reproduced correctly after a few decades of simulations by assuming molecular diffusion and gravitational adjustment only. This indicates that, as expected, the stratification parameters and the molecular diffusivities define the physics. However, it is far from clear why some of the layers in Lake Kivu retain their identity over decades, whereas others seem to continuously transform. By comparing with measurements from 1972 (Newman 1976), we have some indication that the average mixed layer thickness decreased (Schmid et al. 2010). From the more than 300 microstructure profiles, we are not able to identify which layers merge or are newly created. Layer formation, decay, and merging are most probably also affected by background turbulence, as indicated by the absence of layering within an ~2-km horizontal distance to the shore (Sommer et al. 2013).

Another puzzling observation concerns the horizontal coherence of the layering. The detailed observations in Lake Kivu demonstrated remarkably that horizontal coherence is very inhomogeneous with individual mixed layers traceable over horizontal distances of more than ~10 km, whereas other layers did not show the slightest identity even over the shortest distances of less than a few 100 m. Similar coherent diffusive-type staircase layering was also found in the Arctic with horizontal extents of up to ~800 km (Timmermans et al. 2008). The interleaving of large intruding water masses, as present in the Arctic, may also play a role for the large-scale coherency in Lake Kivu.

6. BIOCONVECTION IN LAKES

The question of whether organisms cause mixing in oceans and lakes is a long-standing puzzle (Visser 2007, Leshansky & Pismen 2010). This challenge inspired an enormous laboratory-based research volume, beyond the scope of this review (Guasto et al. 2012), but it initiated only limited studies in lakes. Farmer et al. (1987) performed microstructure measurements in a bay to estimate the turbulence level, expressed by TKE dissipation, to test whether high fish density could

modify the stratification in natural waters. To be effective, organisms must overcome geophysically driven turbulent diffusivities in the stratified ocean interior ($\sim 10^{-5}$ m^2 s^{-1}) or the stratified hypolimnia of lakes ($\sim 10^{-6}$ m^2 s^{-1}). This implies that the products $\overline{L'w'}$ of the eddy sizes L' and velocities w', generated by aquatic organisms, need to overcome those geophysical diffusivities (Kunze et al. 2006). From all known observations so far, it appears that biogenic turbulence does not significantly contribute to mixing or stratification changes (Katija 2012, Wang & Ardekani 2015, Simoncelli et al. 2017). Although Noss & Lorke (2012) showed that swimming zooplankton can significantly enhance TKE dissipation in direct proximity by creating eddies in their wakes and by dragging water along, the generated L' are too short to have a macroscopic effect. The mechanical energy is dissipated in the viscous-diffusive envelope around the organisms, implying that swimming-induced fluctuations in velocity and density are evened out before they are advected.

While mechanical forcing by organisms may be negligible, there is an alternative to propulsion-induced biogenic turbulence. Bioconvection (Pedley & Kessler 1992) can be initiated if the microorganisms induce water movements by locally changing the fluid density, which then finally drives convection (Bearon & Grünbaum 2006). This scenario was demonstrated by Sommer et al. (2017), who studied the upward-swimming purple sulfur bacteria *Chromatium okenii*. These bacteria, with body volumes of V_b and concentrations of C_B, are heavier than ambient water and can mix up to an ~1-m-thick layer in a stratified natural lake (**Figures 1*g*** and **8**). The basic idea is that

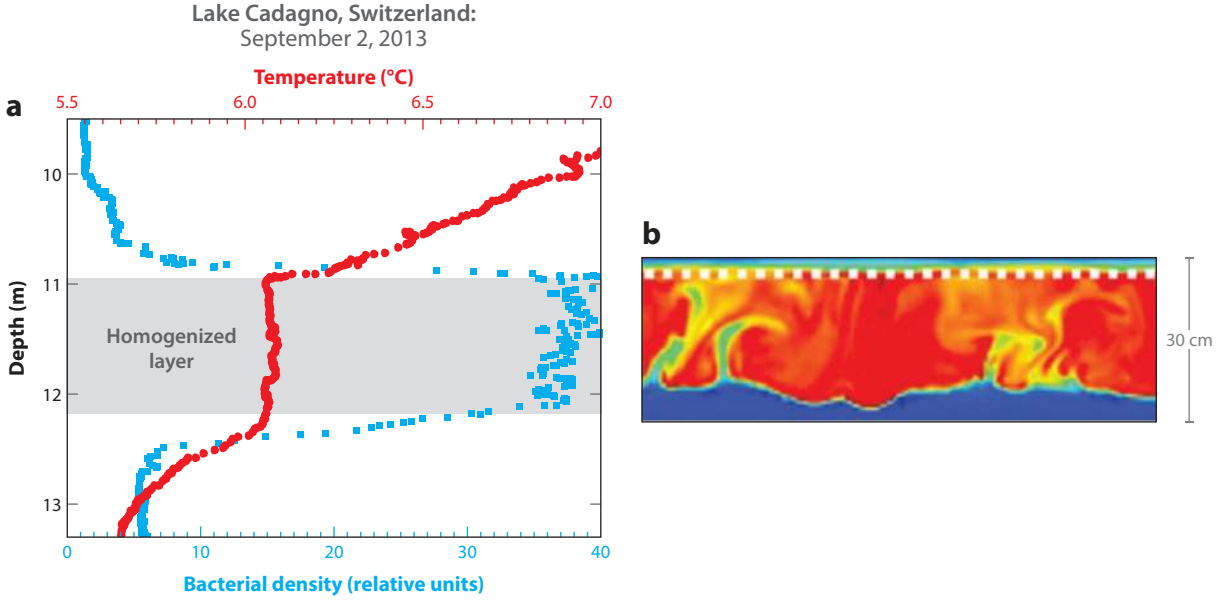

Figure 8

(*a*) Bacteria-induced convection in Lake Cadagno (Switzerland). Temperature (*red*) and bacteria concentration profiles (*blue*) on September 2, 2013, near mid-depth of Lake Cadagno, where autotrophic sulfur bacteria *Chromatium okenii* are densely concentrated at the oxic–anoxic interface. Due to their having a higher density than water and the ability to swim upward, they cause bioconvection and can homogenize a layer (*gray*) more than 1 m thick. (*b*) Direct numerical simulation (DNS) model results showing concentrations of convective plumes in a 30-cm-thick layer that developed after 10 hours of DNS, corresponding to the real in situ conditions in August 2015 (for further detail, see Sommer et al. 2017). At this moment, 45% of the bacterial energy input is dissipated and 55% is converted to potential energy. Figure adapted with permission from Sommer et al. (2017).

the bacteria-induced upward net mass flux $w_B(\rho_b - \rho)(V_b C_B)$ (kg m^{-2} s^{-1}) produces potential energy at a rate of $g\rho^{-1} w_B(\rho_b - \rho)(V_b C_B)$ (W kg^{-1}) (Equation 1), which is identical to the buoyancy flux rate B_* that drives the subsequent convection (Section 1; **Table 1**). The specific conditions found in the lake are $w_B \approx 9 \times 10^{-6}$ m s^{-1} for the upward-swimming velocity, $(\rho_B - \rho)\rho^{-1} \approx 0.15$ for the density excess of the heavy bacteria, and $V_b C_B \approx 2.5 \times 10^{-16}$ m^3 $\times$ 7.5×10^{10} m^{-3} for the nondimensional ratio of the bacteria volume within the water. For these field-based values, the energy input by the upward-swimming bacteria is $B_* \approx 2.5 \times 10^{-10}$ W kg^{-1}. DNSs prove that with this level of energy input, the *C. okenii* are capable not only of maintaining the mixed layer but also of gradually expanding this convective layer to several decimeters in thickness (**Figure 8**), which is consistent with field observations of up to 1.2 m maximum thickness (Sommer et al. 2017). Also, the DNS level of TKE dissipation compared excellently with temperature microstructure estimates in the lake, in the range of 10^{-10} W kg^{-1}, and this closed the TKE balance (Sommer et al. 2017).

This unique observation in a natural environment stimulates various follow-up questions, especially concerning the initiation and relevance of bioconvection. Important net effects of this particular type of bioconvection are that the habitat of the microorganisms is expanded, nutrients are entrained into and distributed over the mixing layer, and the photoautotrophic organisms are evenly exposed to the weak available light. The fascinating question is whether bioconvection provides an evolutionary advantage, and if so, why has this phenomenon not been observed more often? Or has it been overlooked? Many phytoplankton species are denser than water and can swim upward because they are bottom-heavy or exhibit phototactic behavior, and thus they are potentially capable of driving bioconvection. Given the wide range of potential species and their ubiquity, bioconvection potentially may play an important role in plankton distributions and algal blooms.

Directly related to this evolutionary aspect is the practical question regarding the conditions needed for bioconvection to be initiated. Based on the DNS model implemented by Sommer et al. (2017), it should be possible to evaluate all relevant environmental parameters, such as stratification, light, and nutrients to name a few, to understand their role in this rather unique phenomenon in aquatic systems. During summer, the higher *C. okenii* concentrations cause more active bioconvection, which may have a beneficial effect (positive feedback) for the ecological niche required for *C. okenii*.

7. CONCLUSION AND FUTURE DIRECTIONS

This review describes, to our knowledge, the most relevant convective processes observed in lakes (**Figure 1**). For most of these phenomena, mechanistic understanding and quantitative descriptions have to a large extent been reached. Today, the challenge is rather in quantifying how these convective processes shape the physical environment in natural and man-made inland waters and how associated fluxes affect the ecosystems. Specifically, it has not been considered how the different convective processes interact in the lateral direction, which is especially challenging in water bodies of complex natural forms. Lakes are far from homogeneous, and the effect of convective turbulence on horizontal transport in real systems needs to be considered. The technology is now mature enough to apprehend the three-dimensional dynamics of convective processes and associated mixing and net transport. The synergistic use of fast-responding sensors moored or mounted on underwater vehicles or profiling systems, together with remotely sensed earth observations and high-performance computing, will allow researchers to address today's questions from a fluid mechanics viewpoint as well as from an ecosystem perspective.

FUTURE ISSUES

1. The net effects resulting from the interaction between open water and sidearm cooling are largely underexplored. Interplay with other processes (internal waves, wind, nearshore vegetation, etc.) has also been ignored in the past. Along the same line, research is also needed into under-ice convection for inhomogeneous radiation forcing and the subsequent lateral circulation.
2. Research on the near-surface convective layer will favor (*a*) better skin-to-bulk parameterization of the remotely sensed surface temperatures, (*b*) gas exchange relevant for greenhouse gas evasion, and (*c*) inclusion of the surfactant layer into air–water dynamics. All these results will be of high interest for integrative modeling of convective processes.
3. The net transport resulting from boundary mixing and, more specifically, from combined shear-driven convection and pore water convection could provide an integrated view regarding the exchange of constituents, such as oxygen or nutrients, between the lake interior and the sediment.
4. The lateral coherent extent and the formation and temporal development of double-diffusive layering patterns still remain unresolved and poorly understood.

DISCLOSURE STATEMENT

The authors are not aware of any biases that might be perceived as affecting the objectivity of this review.

ACKNOWLEDGMENTS

We thank our colleagues Tobias Jonas, Ilker Fer, Andreas Lorke, Bertram Boehrer, and Tobias Sommer for providing us figures. We are also thankful to Bertram Boehrer, Jeff Carpenter, Georgiy Kirillin, Robert Schwefel, and Hugo Ulloa for comments on an earlier version of the manuscript. With this article we want to honor our long-term field technician Michael Schurter, who was involved in most of the data collected during our lake work, and who unexpectedly passed away during preparation of this publication.

LITERATURE CITED

Adrian R, O'Reilly CM, Zagarese H, Baines SB, Hessen DO, et al. 2009. Lakes as sentinels of climate change. *Limnol. Oceanogr.* 54(6):2283–97

Alavian V, Jirka GH, Denton RA, Johnson MC, Stefan HG. 1992. Density currents entering lakes and reservoirs. *J. Hydraul. Eng.* 118:1464–89

Anati DA, Stiller M. 1991. The post-1979 thermohaline structure of the Dead Sea and the role of double-diffusive mixing. *Limnol. Oceanogr.* 36:342–53

Anati DA, Stiller M, Shasha S, Gat JR. 1987. Changes in the thermo-haline structure of the Dead Sea: 1979–1984. *Earth Planet. Sci. Lett.* 84:109–21

Baines PG. 2001. Mixing in flows down gentle slopes into stratified environments. *J. Fluid Mech.* 443:237–70

Bearon RN, Grünbaum D. 2006. Bioconvection in a stratified environment: experiments and theory. *Phys. Fluids* 18:127102

Becherer JK, Umlauf L. 2011. Boundary mixing in lakes: 1. Modeling the effect of shear-induced convection. *J. Geophys. Res.* 116:C10017

Boehrer B, Dietz S, von Rohden C, Kiwel U, Jöhnk KD, et al. 2009a. Double-diffusive deep water circulation in an iron-meromictic lake. *Geochem. Geophys. Geosyst.* 10:Q06006
Boehrer B, Fukuyama R, Chikita K, Kikukawa H. 2009b. Deep water stratification in deep caldera lakes Ikeda, Towada, Tazawa, Kuttara, Toya and Shikotsu. *Limnology* 10:17–24
Boehrer B, Golmen L, Løvik JE, Rahn K, Klaveness D. 2013. Thermobaric stratification in very deep Norwegian freshwater lakes. *J. Gt. Lakes Res.* 39:690–95
Boehrer B, Schultze M. 2008. Stratification of lakes. *Rev. Geophys.* 46:RG2005
Bouffard D, Perga M-E. 2016. Are flood-driven turbidity currents hot spots for priming effect in lakes? *Biogeosciences* 13:3573–84
Bouffard D, Zdorovennov RE, Zdorovennova GE, Pasche N, Wüest A, Terzhevik AY. 2016. Ice-covered Lake Onega: effects of radiation on convection and internal waves. *Hydrobiologia* 780:21–36
Carmack EC, Gray CBJ, Pharo CH, Daley RJ. 1979. Importance of lake-river interaction on seasonal patterns in the general circulation of Kamloops Lake, British Columbia. *Limnol. Oceanogr.* 24:634–44
Carmack EC, Weiss RF. 1991. Convection in Lake Baikal: an example of thermobaric instability. In *Deep Convection and Deep Water Formation in the Oceans*, ed. PC Chu, JC Gascard, pp. 215–28. Amsterdam: Elsevier
Carpenter JR, Sommer T, Wüest A. 2012a. Simulations of a double-diffusive interface in the diffusive convection regime. *J. Fluid Mech.* 711:411–36
Carpenter JR, Sommer T, Wüest A. 2012b. Stability of a double-diffusive interface in the diffusive convection regime. *J. Phys. Oceanogr.* 42:840–54
Cenedese C, Adduce C. 2010. A new parameterization for entrainment in overflows. *J. Phys. Oceanogr.* 40:1835–50
Chen C-TA, Millero FJ. 1986. Thermodynamic properties for natural waters covering only the limnological range. *Limnol. Oceanogr.* 31:657–62
Chowdhury MR, Wells MG, Howell T. 2016. Movements of the thermocline lead to high variability in benthic mixing in the nearshore of a large lake. *Water Resour. Res.* 52:3019–39
Cole JJ, Prairie YT, Caraco NF, McDowell WH, Tranvik LJ, et al. 2007. Plumbing the global carbon cycle: integrating inland waters into the terrestrial carbon budget. *Ecosystems* 10:172–85
Cortés A, Fleenor WE, Wells MG, de Vicente I, Rueda FJ. 2014. Pathways of river water to the surface layers of stratified reservoirs. *Limnol. Oceanogr.* 59:233–50
Cossu R, Wells MG. 2013. The interaction of large amplitude internal seiches with a shallow sloping lakebed: observations of benthic turbulence in Lake Simcoe, Ontario, Canada. *PLOS ONE* 8:e57444
Crawford GB, Collier RW. 1997. Observations of a deep-mixing event in Crater Lake, Oregon. *Limnol. Oceanogr.* 42:299–306
Crawford GB, Collier RW. 2007. Long-term observations of deepwater renewal in Crater Lake, Oregon. *Hydrobiologia* 574:47–68
Csanady GT. 1975. Hydrodynamics of large lakes. *Annu. Rev. Fluid Mech.* 7:357–86
Davarpanah Jazi S, Wells MG. 2016. Enhanced sedimentation beneath particle-laden flows in lakes and the ocean due to double-diffusive convection. *Geophys. Res. Lett.* 43:10883–90
Deardorff JW. 1970. Convective velocity and temperature scales for the unstable planetary boundary layer and for Rayleigh convection. *J. Atmos. Sci.* 27:1211–13
Ellison TH, Turner JS. 1959. Turbulent entrainment in stratified flows. *J. Fluid Mech.* 6:423–48
Emanuel KA. 1994. *Atmospheric Convection*. New York: Oxford Univ. Press
Emery WJ, Castro S, Wick GA, Schluessel P, Donlon C. 2001. Estimating sea surface temperature from infrared satellite and in situ temperature data. *Bull. Am. Meteorol. Soc.* 82:2773–85
Eugster W, Kling G, Jonas T, McFadden JP, Wüest A, et al. 2003. CO_2 exchange between air and water in an Arctic Alaskan and midlatitude Swiss lake: importance of convective mixing. *J. Geophys. Res.* 108:4362
Fang X, Stefan HG. 1996. Dynamics of heat exchange between sediment and water in a lake. *Water Resour. Res.* 32:1719–27
Farmer DD, Crawford GB, Osborn TR. 1987. Temperature and velocity microstructure caused by swimming fish. *Limnol. Oceanogr.* 32:978–83
Farmer DM. 1975. Penetrative convection in the absence of mean shear. *Q. J. R. Meteorol. Soc.* 101:869–91

Farrow DE, Patterson JC. 1993. On the response of a reservoir sidearm to diurnal heating and cooling. *J. Fluid Mech.* 246:143–61
Fer I, Lemmin U, Thorpe SA. 2002. Winter cascading of cold water in Lake Geneva. *J. Geophys. Res. Oceans* 107(C6):13-1–13-16
Finckh P. 1981. Heat-flow measurements in 17 perialpine lakes. *Geol. Soc. Am. Bull.* 92:452–514
Fink G, Wessels M, Wüest A. 2016. Flood frequency matters: why climate change degrades deep-water quality of peri-alpine lakes. *J. Hydrol.* 540:457–68
Forrest AL, Laval BE, Pieters R, Lim DSS. 2013. A cyclonic gyre in an ice-covered lake. *Limnol. Oceanogr.* 58:363–75
Garaud P. 2018. Double-diffusive convection at low Prandtl number. *Annu. Rev. Fluid Mech.* 50:275–98
Golosov SD, Ignatieva NV. 1999. Hydrothermodynamic features of mass exchange across the sediment–water interface in shallow lakes. *Hydrobiologia* 408/409:153–57
Gregg MC, D'Asaro EA, Riley JJ, Kunze E. 2018. Mixing efficiency in the ocean. *Annu. Rev. Mar. Sci.* 10:443–73
Guasto JS, Rusconi R, Stocker R. 2012. Fluid mechanics of planktonic microorganisms. *Annu. Rev. Fluid Mech.* 44:373–400
Gulati RD, Zadereev ES, Degermendzhi AG, eds. 2017. *Ecology of Meromictic Lakes*. Cham, Switz.: Springer
Henderson SM. 2016. Upslope internal-wave Stokes drift, and compensating downslope Eulerian mean currents, observed above a lakebed. *J. Phys. Oceanogr.* 46:1947–61
Hoare RA. 1966. Problems of heat transfer in Lake Vanda, a density stratified Antarctic lake. *Nature* 210:787–89
Hogg CAR, Marti CL, Huppert HE, Imberger J. 2013. Mixing of an interflow into the ambient water of Lake Iseo. *Limnol. Oceanogr.* 58:579–92
Hughes GO, Gayen B, Griffiths RW. 2013. Available potential energy in Rayleigh–Bénard convection. *J. Fluid Mech.* 729:R3
Huppert HE, Linden PF. 1979. On heating a stable salinity gradient from below. *J. Fluid Mech.* 95(3):431–464
Huppert HE, Turner JS. 1972. Double-diffusive convection and its implications for the temperature and salinity structure of the ocean and Lake Vanda. *J. Phys. Oceanogr.* 2:456–61
Imberger J. 1985. The diurnal mixed layer. *Limnol. Ocean* 30:737–70
Imberger J. 1998. Flux paths in a stratified lake: a review. In *Physical Processes in Lakes and Oceans*, ed. J Imberger, pp. 1–17. Washington, DC: Am. Geophys. Union
Imberger J, Hamblin PF. 1982. Dynamics of lakes, reservoirs, and cooling ponds. *Annu. Rev. Fluid Mech.* 14:153–87
Ivey GN, Winters KB, Koseff JR. 2008. Density stratification, turbulence, but how much mixing? *Annu. Rev. Fluid Mech.* 40:169–84
Jonas T, Terzhevik AY, Mironov DV, Wüest A. 2003a. Radiatively driven convection in an ice-covered lake investigated by using temperature microstructure technique. *J. Geophys. Res.* 108:3183
Jonas T, Wüest A, Eugster W, Stips A. 2003b. Observations of a quasi shear-free lacustrine convective boundary layer: stratification and its implications on turbulence. *J. Geophys. Res.* 108:3328
Katija K. 2012. Biogenic inputs to ocean mixing. *J. Exp. Biol.* 215:1040–49
Kelley DE. 1997. Convection in ice-covered lakes: effects on algal suspension. *J. Plankton Res.* 19:1859–80
Kirillin G, Engelhardt C, Golosov S. 2009. Transient convection in upper lake sediments produced by internal seiching. *Geophys. Res. Lett.* 36:L18601
Kirillin G, Forrest AL, Graves KE, Fischer A, Engelhardt C, Laval BE. 2015. Axisymmetric circulation driven by marginal heating in ice-covered lakes. *Geophys. Res. Lett.* 42:2893–900
Kirillin G, Leppäranta M, Terzhevik A, Granin N, Bernhardt J, et al. 2012. Physics of seasonally ice-covered lakes: a review. *Aquat. Sci.* 74:659–82
Kouraev AV, Zakharova EA, Rémy F, Kostianoy AG, Shimaraev MN, et al. 2016. Giant ice rings on lakes Baikal and Hovsgol: inventory, associated water structure and potential formation mechanism. *Limnol. Oceanogr.* 61:1001–14
Kunze E, Dower JF, Beveridge I, Dewey R, Bartlett KP. 2006. Observations of biologically generated turbulence in a coastal inlet. *Science* 313:1768–70

Laval BE, Morrison J, Potts DJ, Carmack EC, Vagle S, et al. 2008. Wind-driven summertime upwelling in a fjord-type lake and its impact on downstream river conditions: Quesnel Lake and River, British Columbia, Canada. *J. Gt. Lakes Res.* 34:189–203
Laval BE, Vagle S, Potts D, Morrison J, Sentlinger G, et al. 2012. The joint effects of riverine, thermal, and wind forcing on a temperate fjord lake: Quesnel Lake, Canada. *J. Gt. Lakes Res.* 38:540–49
Legg S. 2012. Overflows and convectively driven flows. In *Buoyancy-Driven Flows*, ed. EP Chassignet, C Cenedese, J Verron, pp. 203–39. New York: Cambridge Univ. Press
Lei C, Patterson JC. 2005. Unsteady natural convection in a triangular enclosure induced by surface cooling. *Int. J. Heat Fluid Flow* 26:307–21
Leshansky AM, Pismen LM. 2010. Do small swimmers mix the ocean? *Phys. Rev. E* 82:025301
Linden PF. 1973. The interaction of a vortex ring with a sharp density interface: a model for turbulent entrainment. *J. Fluid Mech.* 60:467–80
Linden PF. 1975. The deepening of a mixed layer in a stratified fluid. *J. Fluid Mech.* 71:385–405
Lorke A, Peeters F, Wüest A. 2005. Shear-induced convective mixing in bottom boundary layers on slopes. *Limnol. Oceanogr.* 50:1612–19
Lorke A, Umlauf L, Mohrholz V. 2008. Stratification and mixing on sloping boundaries. *Geophys. Res. Lett.* 35:L14610
Lorrai C, Umlauf L, Becherer JK, Lorke A, Wüest A. 2011. Boundary mixing in lakes: 2. Combined effects of shear- and convectively induced turbulence on basin-scale mixing. *J. Geophys. Res.* 116:C10018
Mao Y, Lei C, Patterson JC. 2010. Unsteady near-shore natural convection induced by surface cooling. *J. Fluid Mech.* 642:213–33
Matthews PC, Heaney SI. 1987. Solar heating and its influence on mixing in ice-covered lakes. *Freshw. Biol.* 18:135–49
Mellado JP. 2017. Cloud-top entrainment in stratocumulus clouds. *Annu. Rev. Fluid Mech.* 49:145–69
Miesch MS, Toomre J. 2009. Turbulence, magnetism, and shear in stellar interiors. *Annu. Rev. Fluid Mech.* 41:317–45
Mironov D, Terzhevik A, Kirillin G, Jonas T, Malm J, Farmer D. 2002. Radiatively driven convection in ice-covered lakes: observations, scaling, and a mixed layer model. *J. Geophys. Res.* 107:7-1–7-16
Monismith SG, Imberger J, Morison ML. 1990. Convective motions in the sidearm of a small reservoir. *Limnol. Oceanogr.* 35:1676–702
Mortimer CH, Mackereth FJH. 1958. Convection and its consequences in ice-covered lakes. *SIL Proc. 1922–2010* 13:923–32
Moum JN, Perlin A, Klymak JM, Levine MD, Boyd T, Kosro PM. 2004. Convectively driven mixing in the bottom boundary layer. *J. Phys. Oceanogr.* 34:2189–202
Newman FC. 1976. Temperature steps in Lake Kivu: a bottom heated saline lake. *J. Phys. Oceanogr.* 6:157–63
Noss C, Lorke A. 2012. Zooplankton induced currents and fluxes in stratified waters. *Water Qual. Res. J.* 47:276–86
Parker G, Garcia M, Fukushima Y, Yu W. 1987. Experiments on turbidity currents over an erodible bed. *J. Hydraul. Res.* 25:123–47
Pedley TJ, Kessler JO. 1992. Hydrodynamic phenomena in suspensions of swimming microorganisms. *Annu. Rev. Fluid Mech.* 24:313–58
Peeters F, Finger D, Hofer M, Brennwald M, Livingstone DM, Kipfer R. 2003. Deep-water renewal in Lake Issyk-Kul driven by differential cooling. *Limnol. Oceanogr.* 48:1419–31
Peeters F, Straile D, Lorke A, Ollinger D. 2007. Turbulent mixing and phytoplankton spring bloom development in a deep lake. *Limnol. Oceanogr.* 52:286–98
Peltier WR, Caulfield CP. 2003. Mixing efficiency in stratified shear flows. *Annu. Rev. Fluid Mech.* 35:135–167
Pieters R, Lawrence GA. 2009. Effect of salt exclusion from lake ice on seasonal circulation. *Limnol. Oceanogr.* 54:401–12
Powers SM, Hampton SE. 2016. Winter limnology as a new frontier. *Limnol. Oceanogr. Bull.* 25:103–8
Råman Vinnå L, Wüest A, Zappa M, Fink G, Bouffard D. 2018. Tributaries affect the thermal response of lakes to climate change. *Hydrol. Earth Syst. Sci.* 22:31–51
Rippeth TP, Fisher NR, Simpson JH. 2001. The cycle of turbulent dissipation in the presence of tidal straining. *J. Phys. Oceanogr.* 31:2458–71

Rodgers GK. 1965. The thermal bar in the Laurentian Great Lakes. In *Proceedings of the 8th Conference on Great Lakes Research*, pp. 358–63. Ann Arbor, MI: Inst. Sci. Technol., Univ. Michigan
Rutgersson A, Smedman A, Sahlée E. 2011. Oceanic convective mixing and the impact on air-sea gas transfer velocity. *Geophys. Res. Lett.* 38:L02602
Sánchez X, Roget E. 2007. Microstructure measurements and heat flux calculations of a triple-diffusive process in a lake within the diffusive layer convection regime. *J. Geophys. Res. Oceans* 112:C02012
Scheifele B, Pawlowicz R, Sommer T, Wüest A. 2014. Double diffusion in saline Powell Lake, British Columbia. *J. Phys. Oceanogr.* 44:2893–908
Schmid M, Budnev NM, Granin NG, Sturm M, Schurter M, Wüest A. 2008. Lake Baikal deepwater renewal mystery solved. *Geophys. Res. Lett.* 35:L09605
Schmid M, Busbridge M, Wüest A. 2010. Double-diffusive convection in Lake Kivu. *Limnol. Oceanogr.* 55:225–38
Schmid M, Lorke A, Dinkel C, Tanyileke G, Wüest A. 2004a. Double-diffusive convection in Lake Nyos, Cameroon. *Deep Sea Res. Part I* 51:1097–111
Schmid M, Tietze K, Halbwachs M, Lorke A, McGinnis DF, Wüest A. 2004b. How hazardous is the gas accumulation in Lake Kivu? Arguments for a risk assessment in light of the Nyiragongo Volcano eruption of 2002. *Acta Vulcanol.* 14–15:115–22
Schmitt RW. 1994. Double diffusion in oceanography. *Annu. Rev. Fluid Mech.* 26:255–85
Schwefel R, Gaudard A, Wüest A, Bouffard D. 2016. Effects of climate change on deep-water oxygen and winter mixing in a deep lake (Lake Geneva): comparing observational findings and modeling. *Water Resour. Res.* 52:8811–26
Shay TJ, Gregg MC. 1986. Convectively driven turbulent mixing in the upper ocean. *J. Phys. Oceanogr.* 16:1777–98
Shibley NC, Timmermans ML, Carpenter JR, Toole JM. 2017. Spatial variability of the Arctic Ocean's double-diffusive staircase. *J. Geophys. Res. Oceans* 122:980–94
Simoncelli S, Thackeray SJ, Wain DJ. 2017. Can small zooplankton mix lakes? *Limnol. Oceanogr. Lett.* 2:167–76
Simpson JH, Brown J, Matthews J, Allen G. 1990. Tidal straining, density currents, and stirring in the control of estuarine stratification. *Estuaries Coasts* 13:125–32
Soloviev A, Lukas R. 2014. *The Near-Surface Layer of the Ocean: Structure, Dynamics and Applications*. Dordrecht, Neth.: Springer
Sommer T, Carpenter JR, Schmid M, Lueck RG, Schurter M, Wüest A. 2013. Interface structure and flux laws in a natural double-diffusive layering. *J. Geophys. Res. Oceans* 118:6092–106
Sommer T, Carpenter JR, Wüest A. 2014. Double-diffusive interfaces in Lake Kivu reproduced by direct numerical simulations. G*eophys. Res. Lett*. 41:5114–21
Sommer T, Danza F, Berg J, Sengupta A, Constantinescu G, et al. 2017. Bacteria-induced mixing in natural waters. *Geophys. Res. Lett.* 44:9424–32
Steinhorn I. 1985. The disappearance of the long term meromictic stratification of the Dead Sea. *Limnol. Oceanogr.* 30:451472
Stern ME. 1960. The "salt-fountain" and thermohaline convection. *Tellus* 12:172–75
Stommel H, Arons AB, Blanchard D. 1956. An oceanographical curiosity—the perpetual salt fountain. *Deep Sea Res.* 3:152–53
Strøm K. 1962. Trapped sea water. *New Sci.* 274:384–86
Sturman JJ, Oldham CE, Ivey GN. 1999. Steady convective exchange flows down slopes. *Aquat. Sci.* 61:260–78
Sutherland BR, Gingras MK, Knudson C, Steverango L, Surma C. 2018. Particle-bearing currents in uniform density and two-layer fluids. *Phys. Rev. Fluids* 3(2):023801
Tanaka M, Girard G, Davis R, Peuto A, Bignell N. 2001. Recommended table for the density of water between 0 °C and 40 °C based on recent experimental reports. *Metrologia* 38:301–9
Tedford EW, MacIntyre S, Miller SD, Czikowsky MJ. 2014. Similarity scaling of turbulence in a temperate lake during fall cooling. *J. Geophys. Res. Oceans* 119:4689–713
Timmermans M-L, Toole J, Krishfield R, Winsor P. 2008. Ice-tethered profiler observations of the double-diffusive staircase in the Canada Basin thermocline. *J. Geophys. Res. Oceans* 113:C00A02
Tivey MA, de Ronde CEJ, Tontini FC, Walker SL, Fornari DJ. 2016. A novel heat flux study of a geothermally active lake—Lake Rotomahana, New Zealand. *J. Volcanol. Geotherm. Res.* 314:95–109

Toffolon M, Wüest A, Sommer T. 2015. Minimal model for double diffusion and its application to Kivu, Nyos, and Powell Lake. *J. Geophys. Res. Oceans* 120:6202–24
Townsend AA. 1964. Natural convection in water over an ice surface. *Q. J. R. Meteorol. Soc.* 90:248–59
Turner JS. 1974. Double-diffusive phenomena. *Annu. Rev. Fluid Mech.* 6:37–54
Turner JS. 1986. Turbulent entrainment: the development of the entrainment assumption, and its application to geophysical flows. *J. Fluid Mech.* 173:431–71
Ulloa H, Wüest A, Bouffard D. 2018. Mechanical energy budget and mixing efficiency for a radiatively heated ice-covered waterbody. *J. Fluid Mech.* 852:R1
Vehmaa A, Salonen K. 2009. Development of phytoplankton in Lake Pääjärvi (Finland) during under-ice convective mixing period. *Aquat. Ecol.* 43:693–705
Velmurugan V, Srithar K. 2008. Prospects and scopes of solar pond: a detailed review. *Renew. Sustain. Energy Rev.* 12:2253–63
Verburg P, Antenucci JP, Hecky RE. 2011. Differential cooling drives large-scale convective circulation in Lake Tanganyika. *Limnol. Oceanogr.* 56:910–26
Verburg P, Hecky RE, Kling H. 2003. Ecological consequences of a century of warming in Lake Tanganyika. *Science* 301:505–7
Visser AW. 2007. Biomixing of the oceans? *Science* 316:838–39
von Rohden C, Boehrer B, Ilmberger J. 2010. Evidence for double diffusion in temperate meromictic lakes. *Hydrol. Earth Syst. Sci.* 14:667–74
Wang S, Ardekani AM. 2015. Biogenic mixing induced by intermediate Reynolds number swimming in stratified fluids. *Sci. Rep.* 5:17448
Weinberger H. 1964. The physics of the solar pond. *Sol. Energy* 8:45–56
Wells M, Cenedese C, Caulfield CP. 2010. The relationship between flux coefficient and entrainment ratio in density currents. *J. Phys. Oceanogr.* 40:2713–27
Wells M, Nadarajah P. 2009. The intrusion depth of density currents flowing into stratified water bodies. *J. Phys. Oceanogr.* 39:1935–47
Wilson AT, Wellman HW. 1962. Lake Vanda: an Antarctic lake. *Nature* 196:1171–73
Wilson RC, Hook SJ, Schneider P, Schladow SG. 2013. Skin and bulk temperature difference at Lake Tahoe: a case study on lake skin effect. *J. Geophys. Res. Atmos.* 118:10332–46
Woods AW. 2010. Turbulent plumes in nature. *Annu. Rev. Fluid Mech.* 42:391–412
Wüest A, Carmack EC. 2000. A priori estimates of mixing and circulation in the hard-to reach water body of Lake Vostok. *Ocean Model.* 2:29–43
Wüest A, Lorke A. 2003. Small-scale hydrodynamics in lakes. *Annu. Rev. Fluid Mech.* 35:373–412
Wüest A, Piepke G, Halfman JD. 1996. Combined effects of dissolved solids and temperature on the density stratification of Lake Malawi (East Africa). In *The Limnology, Climatology and Paleoclimatology of the East African Lakes*, ed. TC Johnson, EO Odada, pp. 183–202. New York: Gordon Breach
Wüest A, Ravens TM, Granin NG, Kocsis O, Schurter M, Sturm M. 2005. Cold intrusions in Lake Baikal—direct observational evidence for deep water renewal. *Limnol. Oceanogr.* 50:184–96
Wüest A, Sommer T, Schmid M, Carpenter JR. 2012. Diffusive-type of double diffusion in lakes—a review. In *Environmental Fluid Mechanics: Memorial Volume in Honour of Prof. Gerhard H. Jirka*, ed. W Rodi, M Uhlmann, pp. 271–84. Boca Raton, FL: CRC
Zilitinkevĭc SS. 1991. *Turbulent Penetrative Convection*. Adelshot, UK: Avebury

Annual Review of
Fluid Mechanics

Volume 51, 2019

Contents

Indexes

Errata

An online log of corrections to *Annual Review of Fluid Mechanics* articles may be found at http://www.annualreviews.org/errata/fluid